LAPPEENRANTA UNIVERSITY OF TECHNOLOGY
LUT School of Energy Systems
Mechanical Engineering

Miro Ahlfors

DISTORTION AND INTERNAL WARPING TORSION OF A DOUBLE SYMMETRIC HOLLOW SECTION

Examiners: Professor Timo Björk
D. Sc. Timo Nykänen

ABSTRACT

Lappeenranta University of Technology
LUT School of Energy Systems
Mechanical Engineering

Miro Ahlfors

Distortion and internal warping torsion of a double symmetric hollow section

Master's Thesis

2015

54 pages, 31 figures, 1 table, 2 appendices

Examiners: Professor Timo Björk
D. Sc. Timo Nykänen

Keywords: cross-sectional distortion, warping, box girder, uniform torsion, non-uniform torsion, structural hollow section

This thesis is made in cooperation with Laboratory of Steel Structures and the steel company SSAB. Maximization of the benefits of high-strength steel usually requires the usage of thin wall thicknesses. This means the failures related to buckling, distortion and warping stand out. One must be aware of these phenomena to design thin-walled structures stressed with forces such as torsional loading. It is also important to take into account small stress ranges when evaluating the accurate fatigue strength of structures.

The objective of this thesis is to clarify the theory of the uniform and non-uniform torsion. This paper focuses on warping due to the non-uniform torsion in double symmetric box girder and structural hollow section. The arisen stress states are explained and researched using the finite element method.

Another research target is the distortion in double symmetric box girder due to torsion, and the restraining effect of transverse diaphragms at the load end. Multiple transverse diaphragms are used to study more efficient restraining against warping and distortion than a common one end plate structure.

TIIVISTELMÄ

Lappeenrannan teknillinen yliopisto
LUT School of Energy Systems
Konetekniikan koulutusohjelma

Miro Ahlfors

Kaksoissymmetrisen kotelopalkin vinoutuminen ja estetty vääntö

Diplomityö

2015

54 sivua, 31 kuvaa, 1 taulukko, 2 liitettä

Tarkastajat: Professori Timo Björk

Hakusanat: poikkileikkauksen vinoutuminen, vapaa vääntö, estetty vääntö, haarukkapuomi, rakenneputki

Tämä tutkimus on tehty yhteistyössä Lappeenrannan teknillisen yliopiston Teräsrakenteiden laboratorion ja SSAB teräsyhtiön kanssa. Lujia teräksiä käytettäessä parhaan hyödyn aikaansaamiseksi on usein ohutlevyrakenteiden käyttö suotavaa niiden kevyen rakenteen ansiosta. Tällöin vaurioilmiöt johtuen paikallisesta lommahduksesta, poikkileikkauksen vinoutumisesta, vääristymisestä ja käyristymisestä korostuvat. Suunnittelijan tulee olla tietoinen niistä ja ymmärtää kyseiset ilmiöt suunnitellessaan ohutlevyrakenteita, jotka joutuvat kuormituksessa esimerkiksi väännön alaisiksi. Siten tarkan väsymiskestävyyden arvioimisessa on syytä ottaa huomioon kyseisten ilmiöiden aiheuttamat pienetkin jännitysvaihtelut.

Tämän diplomityön tavoitteena on selvittää puhtaan ja estetyn väännön erot ja seuraukset. Työssä keskitytään estetyn väännön aiheuttamaan primääriseen ja sekundääriseen käyristymiseen kaksoissymmetrisissä kotelorakenteissa ja rakenneputkissa. Syntyvät jännitystilat ovat selitetty ja havainnollistettu tutkimuksessa tehdyillä elementtimalleilla.

Toinen tärkeä kohde on väännöstä johtuva vinoutuminen kaksoissymmetrisessä kotelopalkissa ja sen estäminen poikittaisilla jäykistelevyillä palkin ulkoisen vääntökuorman vaikutuspäädyssä. Työssä tutkitaan kuinka lisäksi toisen jäykistelevyn sijoittaminen palkin sisälle estää vinoutumista ja maadoittaa käyristymistä verrattuna yleisesti käytettyyn pelkkään päätylevyyn.

ACKNOWLEDGEMENTS

First honorable mentions go to LUT Laboratory of Steel Structures and steel company SSAB, for providing me with this interesting and challenging thesis topic. Especially, I want to thank Professor Timo Björk from Lappeenranta University of Technology, who supervised me and blessed me with his great knowledge. My compliments also to the entire staff of Department of Steel Structures, especially to Timo Nykänen for good words of advice.

All loving thanks to my family and fellow students for the physical and mental support. Thank you to everyone who was involved in this thesis.

Lappeenranta, February of 2015
Miro Ahlfors

TABLE OF CONTENTS

ABSTRACT
TIIVISTELMÄ
ACKNOWLEDGEMENTS
TABLE OF CONTENTS
SYMBOLS AND ABBREVIATIONS

1 INTRODUCTION 9
1.1 Main objectives 9
1.2 Earlier research 10
1.3 Limitations of the study 10
2 LITERATURE REVIEW 11
2.1 Thin-walled structures 11
2.2 Basic theory of torsion 11
2.2.1 Uniform and warping torsion 12
2.2.2 Bimoment 16
2.3 Distortional forces 18
2.4 Primary shear stresses 20
2.5 Warping stresses 20
2.5.1 Warping constant of a single-cell closed section 22
2.6 Secondary warping 22
3 RESEARCH METHODS 25
3.1 Load end variations 25
3.2 Support variations 27
3.2.1 Effective notch stress approach 27
3.3 Rubin’s theory about torsion of structural hollow sections 28
4 RESULTS 30
4.1 The effect of the intermediate diaphragm on the distortion 30
4.2 Warping in the structural hollow section 35

4.3 Results from the effective notch stress approach 40
4.4 Rubin's analytical method for primary warping 43
5 DISCUSSION 44
5.1 Future research 46
6 SUMMARY 48
REFERENCES 49

APPENDIXES

Appendix I: Calculations of the sectional properties and warping stresses by Rubin's analytical method
Appendix II: Distribution of warping function in the structural hollow sections by AGIFAP

SYMBOLS AND ABBREVIATIONS

A	Area of a cross-section	[mm^2]
A_0	Area enclosed by a profile	[mm^2]
B	External breadth of a hollow section	[mm]
b	Breadth of a center line dimension of a hollow section	[mm]
b_n	Breadth of a single element	[mm]
E	Young's modulus	[MPa]
e	Distance between pair of moments	[mm]
F_f	Internal flange load	[N]
F_w	Internal web load	[N]
G	Shear modulus	[MPa]
H	External height of a hollow section	[mm]
h	Height of a center line dimension of a hollow section	[mm]
I_t	Torsional inertia constant	[mm^4]
I_{ts}	Secondary torsional constant	[mm^4]
I_{xx}	Section property about x-axis	[mm^4]
I_{yy}	Section property about y-axis	[mm^4]
I_ω	Warping constant	[mm^6]
$I_{\omega s}$	Secondary warping constant	[mm^6]
k	Torsion characteristic	$[\frac{1}{mm}]$
L	Length of a beam	[mm]
l_0	Factor of a maximum bimoment	[mm]
M	Moment	[Nmm]
M_t	External total torsion moment	[mm]
M_{st}	St. Venant torsion	[Nmm]
M_{DS}	Warping torsion moment	[Nmm]
M_x	Bending moment about cross-sectional x-axis	[Nmm]
M_y	Bending moment about cross-sectional y-axis	[Nmm]
M_{ws}	Secondary warping torsion moment	[Nmm]
M_ω	Bimoment	[Nmm^2]

P	Single load	[N]
r	Corner radius of center line of a hollow section	[mm]
r_t	Normal distance from reference plate to shear center	[mm]
S	Point of a shear center	[-]
s	Line segment	[mm]
S_ω	Sectorial static moment	[mm^4]
t	Wall thickness	[mm]
t_{max}	Maximum wall thickness	[mm]
V	Transverse shear force	[N]
x, y, z	Coordinates	[-]
κ	Factor of a secondary torsion moment	[-]
ν	Poisson's ratio	[-]
σ_ω	Warping stress	[MPa]
τ_{st}	St. Venant shear stress	[MPa]
$\tau_{st,closed}$	Shear stress in closed profile from St. Venant torsion	[MPa]
$\tau_{st,open}$	Shear stress in open profile from St. Venant torsion	[MPa]
τ_ω	Warping shear stress	[N]
ϕ	Torsion angle	[rad]
ω	Warping function, sectorial coordinate	[mm^2]
ω_0	Value of the sectorial coordinate at the starting point	[mm^2]

AGIFAP	Advanced graphical interactive frame analysis package
BEF	Beam on elastic foundation
EN	European standards
ENS	Effective notch stress
FE	Finite element
FEA	Finite element analysis
RHS	Rectangular hollow section
SFS	Finnish standards association
SHS	Square hollow section

1 INTRODUCTION

The development of high-strength steel has led to using them more in beam structures. Such as booms of cranes are one of the most significant applications of the high-strength steel. A beam is typically under different force modes such as bending, torsion, and shear and distortion forces. In order to take full advantage of the properties of high-strength steel it is recommended to use thin-walled structures. However, when using thin-walled beams one must be aware of failure cases which are highlighted. Common failures due to torsion are local buckling and distortional deformations.

Torsional warping is a known phenomenon in beams with an open profile and closed profiles with non-zero warping rigidity, such as rectangular and trapezoidal cross-section. Normally primary warping is considered negligible for beams with a closed profile, but also minor stress amplitudes might be noteworthy for accurate fatigue strength analysis.

In this thesis, primary warping causes mainly membrane stress and secondary warping arises due to the individual twisting of the flange or web plate causing linearly over the thickness distribute stress in those members. The names of these concepts are mixed in some publications, as the primary warping itself is called to cause secondary stresses.

1.1 Main objectives

In this thesis, beams with closed profile are studied. The main objective is to clarify how warping stresses, primary and secondary, form in beams with double symmetric thin-walled rectangular sections due to the eccentric loading and how these stresses react when only pure torsional loading is applied. Beams with idealized square cross-section have zero warping rigidity, because the warping deflections due to twisting are balanced by the warping deflections due to shear straining. Nevertheless, the secondary warping arises due to twisting of the flange and web plates, even if only pure torsion is applied. These secondary stresses are studied and compared with a beam made of RHS (rectangular hollow section).

It was also found that ideal square cross-section gets axially deformed due to the pure torsion loading, which causes axial stress similar to primary warping stress, although the warping

constant for square cross-section is zero. This phenomenon has been studied in this thesis and analyzed how bending radius of the SHS (square hollow section) affects in this case.

These stresses, especially secondary warping stresses, are negligible for ultimate capacity assuming the structure is behaving as a ductile manner. It's important to understand the phenomenon behind these relatively small stress states, when considering the structure relative to its fatigue durability.

In this study, finite element models (FE-models) are modeled with the product of Siemens Femap (finite element modeling and post processing) version 11.1.1. Nx Nastran V9.0 is used as a finite element solver for linear static analyses.

1.2 Earlier research

Earlier studies proved that the second diaphragm, after some distance from the diaphragm of the load end, restrained the distortion more effectively than in the case of only one diaphragm. In consequence warping stresses and transversal bending stresses due to the distortion decreased. This statement is presented in the publication named by Designing of a box girder against distortion and torsional load, and is written in Finnish.

1.3 Limitations of the study

This thesis concentrates on the stress states and deformation forms due to the external torsion loading. Only closed rectangle profiles are studied, and a square profile is under closer examination. The phenomena behind the uniform and non-uniform torsion are explained and illustrated by the analyses.

The main parts of the structure are ends of the beam. First is the load end and the other is the fixed end of the beam. Effects of the second diaphragm, such as restraining of the warping and distortion deformations are studied. When a beam is loaded by pure torsion the distortion does not happen, but fixed end prevents axial deformation so warping stresses arises so that maximum value locates in the fixed end of the beam. In this study simple FE-models are analyzed and also more complicated models using ENS-approach (effective notch stress approach) to illustrate the effects at the weld roots and toes and the importance of fatigue strength analysis.

2 LITERATURE REVIEW

In order to understand the behavior of the beam subjected to external eccentric loading, a few basic theories of torsion should be considered. The next chapters will describe the difference between uniform and non-uniform torsion, and how the warping arises due to the non-uniform torsion, when eccentric loading causes bimoment. Especially for the thin-walled hollow section beams the distortional forces that arise due to the eccentric loading should be taken into account.

2.1 Thin-walled structures

Typically cold-formed structure members are manufactured from thin and cold-rolled steel sheet. These structures are called thin-walled structures. Thin-walled structures and their combinations with other steel structures can be claimed as one of the most developed sector of steel structures. Light-weight and economical construction favors the cold-formed thin-walled structures. Their stiffness and weight-carrying capacity in relation to their dead weight are excellent, because the shape and geometry of the cross-section and strength class of the material can be chosen to best suit the application. Also the light-weight of the thin-walled structures is superior in handling and lifting situations. (Martikainen, 2010, p. 141.)

Slenderness of the cross-section parts of thin-walled structures is considerable, because of small wall thickness. Therefore, buckling is a common phenomenon in the plates of thin-walled members. (Martikainen, 2010, p. 141.)

2.2 Basic theory of torsion

When choosing a cross-section of a beam torsional loading has an important influence over maximum efficiency. I- and H-shaped sections have particularly poor resistance against torsion compared with a tubular member. This is one reason why torsional effects must be taken into account in the design. (Nethercot & Salter, 1989, p. 2.)

A beam will be exposed to additional stresses due to torsion when the resultant of the applied forces does not pass through the shear center of the section. The shear center of a cross-section is on the axial axis of the beam about which the cross-section would twist if torsion

is applied on the beam. Generally, twisting will not happen if the transverse resultant force acts trough the shear center, and so the torsional stresses do not occur. (Nethercot & Salter, 1989, p. 3.)

Thin-walled structures should be taken into consideration in their analysis and design. In a thin-walled beam the shear stresses and strains are much higher compared with those in a solid rectangular beam. So this takes issue with the usual assumption of bending theory, wherein the plane sections remain plane over the entire cross-section of a rectangular beam. (Murray, 1986, p. 1.)

2.2.1 Uniform and warping torsion

The total resistance of a beam to torsion is summarized of two components known as uniform torsion and warping torsion, as seen in figure 1. When warping is involved the beam is in a state of non-uniform torsion. The angle of twist is linear along the beam due to uniform torsion. (Nethercot & Salter, 1989, p. 3.) Non-uniform torsion is sometimes also referred as Vlasov torsion. (Rautaruukki, 1987, p. 150.)

When a certain kind of thin-walled structure is applied with a torsional load there is a warping of the cross-section. The term warping is defined as the out-of-plane distortion of the cross-section of a beam in the direction of the longitudinal axis. Warping can be mostly restrained by introducing direct stresses in the longitudinal direction and shear stresses in the cross-section. These stresses are the warping stresses and the symbols are σ_ω and τ_ω, that can be seen in figure 1(c). The warping is prevented in that structure by, for example, a thick plate welded to left end. Therefore it is found to be much stiffer than the structure seen in figure 1(b). (Murray, 1986, p. 3.)

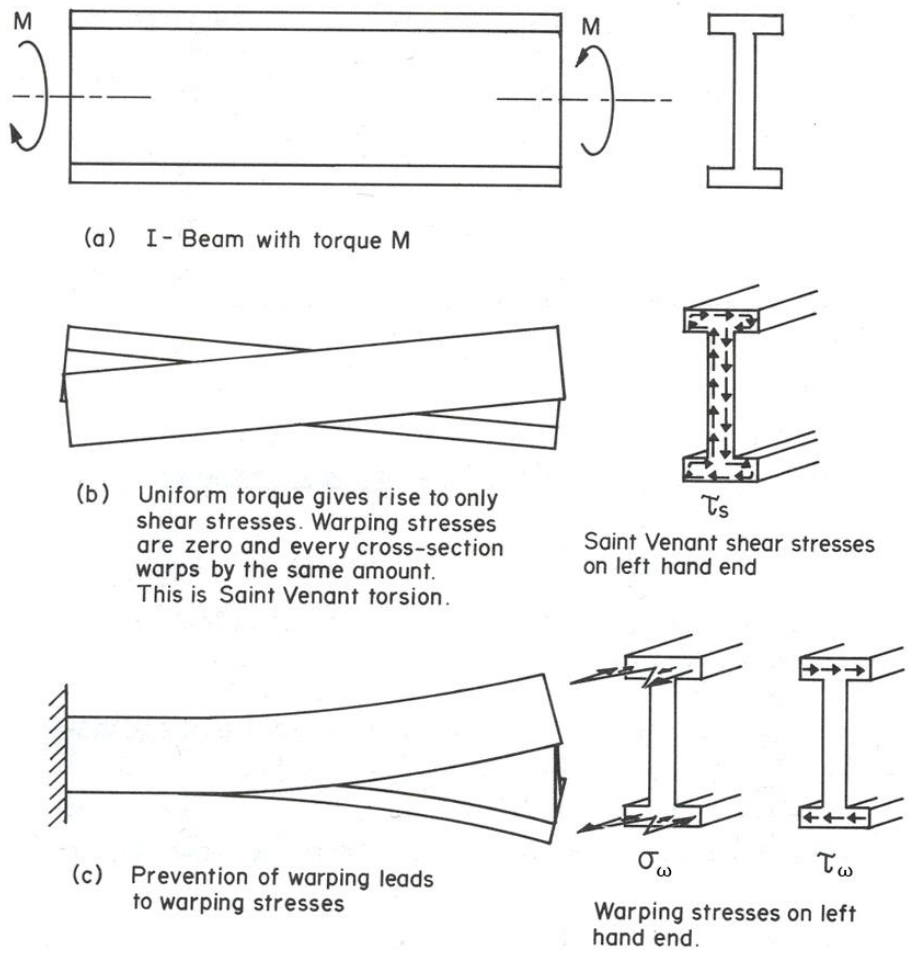

Figure 1. St. Venant and warping torsion in an I-shaped beam (Murray, 1986, p. 3).

Thin-walled open cross-section beams have low torsional stiffness because of the open cross-section and small wall thickness. In extreme cases, the torsional moment will transfer entirely according to the St. Venant torsion or the warping torsion theory. In practice torsion is mix of these two components. (Rautaruukki, 1987, p. 150.)

Theory of the St. Venant torsion assumes that the applied torque is resisted by shear stresses distributed throughout the cross-section, and the rate of change of the angle of twist is constant along the beam, if a torsion moment is applied at the ends of a beam and the cross-section is constant. The relation of the torque to the twist per unit length is equal to the torsional rigidity of the beam. The torsional rigidity is defined by GI_t, where G is the shear modulus and I_t is the torsional constant. Unlike St. Venant torsion, the rate of change of the angle of twist varies along the length of the beam due to the warping torsion, as shown in

figure 1(c) where the left end is fixed and the torque applied end is free to warp. (Nethercot & Salter, 1989, p. 3-5.)

Hence the axial deformations due to warping of the flanges vary along the length of the beam. Normal and shear stresses are generated which are added to those stresses due to the bending and pure torsion. These added stresses are resisted by the warping rigidity EI_ω, where E is Young's modulus of elasticity and I_ω is the warping constant. (Nethercot & Salter, 1989, p. 5.)

The beam is mostly in the state of uniform torsion, if the torsional rigidity, GI_t, is very large compared with the warping rigidity, EI_ω. This kind of section profiles are closed sections, angles, flat plates, T-sections and different sections consisting of a series of plates which radiate from a common point, if only primary warping is discussed. Vice versa, if the warping rigidity is much larger compared with torsional rigidity, the beam will be in a state of the warping torsion. Between these two cases, the beam can also be in the state of non-uniform and uniform. Most of the open sections behave in this manner except for above-mentioned open sections. In this case, the combination of the uniform and warping torsions resists the loading. (Nethercot & Salter, 1989, p. 5.)

One way to predict which torsion case is dominant, is to calculate parameter k as follows

$$k = \sqrt{\frac{G\ I_t}{E\ I_\omega}} \tag{1}$$

Next approximate assumption can be made if:

$kL > 15$, the state of uniform torsion is dominant.
$kL \leq 0{,}7$, the state of warping torsion is dominant.
$0{,}7 < kL \leq 15$, both states of torsion should be taken account.

where L is a length of the beam. (Rautaruukki, 1987, p. 151.)

The effect of warping must be taken into account especially with thin-walled cross-sections loaded by torsion. The theory presented by Vlasov is used to solve such problems with analytical methods. Also, the analogy between second order beam theory and torsion with warping is often used, which is discussed in detail below. The warping takes place mainly at the location of concentrated torsion moments, expect for free beam ends, and in points where warping of cross-section is restrained. (Murín, 2008, p. 2716.)

Noticeable warping is assumed to occur only in the open cross-sections, and for the closed form cross-sections the warping is assumed to be insignificant. (Murín, 2008, p. 2716.) According to the SFS-EN 1993-1-1 (Eurocode 3: Part 1-1):

"As a simplification, in the case of a member with a closed hollow cross-section, such as a structural hollow section, it may be assumed that the effects of torsional warping can be neglected. Also as a simplification, in the case of a member with open cross-section, such as I or H, it may be assumed that the effects of St. Venant torsion can be neglected." (SFS-EN 1993-1-1, 2005, p. 52.)

However, the results of theoretical studies have shown that the effect of warping should be taken into account also in cases of torsion of the beams with a closed profile. (Murín, 2008, p. 2716.) In addition, SFS-EN 1993-1-1 (Eurocode 3: Part 1-1) and other similar design guides are concerning the structures subjected only to the static loading. In the case of fatigue design, the warping must be considered also in case of closed cross-section, especially if high strength steel is used, because it recalls for more precisely performed fatigue analyses. (Björk, 2015.)

When a square cross-section is loaded at one corner by the load *P* as seen in figure 2, the load *P* can be formed from the four sets of loads as described in the lower pictures. In the case of the first three sets, those are axial loading and bending moments about the two axes, the plane sections remains plane over the entire cross-section of the beam. In the fourth loading case the cross-section does not remain plane but warps. This set of stresses are warping stresses. (Murray, 1986, p. 5-6.)

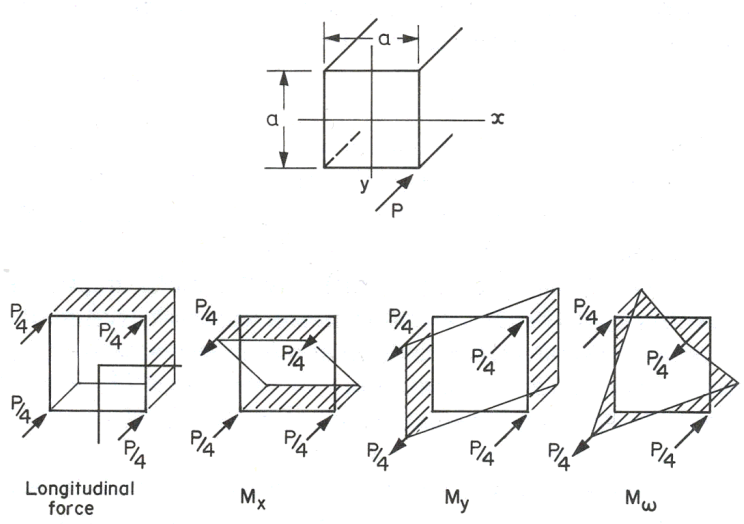

Figure 2. Single load P formed from the four sets of loads (Murray, 1986, p. 5).

The axial stress σ_z at a point (x,y) is the sum of each four sets. Thus

$$\sigma_z = \frac{P}{A} + \frac{M_x y}{I_{xx}} + \frac{M_y x}{I_{yy}} + \frac{M_\omega \omega}{I_\omega} \tag{2}$$

where first term is the axial normal stress, where P is a single load and A is the area of the cross-section. The second term is bending stress due to the bending M_x about the cross-sectional x-axis and the third term due to the bending M_y about the cross-sectional y-axis. I_{xx} and I_{yy} are sectional properties about x- and y-axis. The last term is the longitudinal warping stress σ_ω, where M_ω is bimoment, ω is the warping function and I_ω is the warping constant of the section. (Murray, 1986, p. 6.)

2.2.2 Bimoment

The last set of loads is bimoment, when the single axial load is divided into the four sets of loads as stated in the last section. The bimoment will cause distortions of the cross-section parallel to the longitudinal axis of the beam and a twisting of the beam about its longitudinal axis. This twisting of each plate results in a set of shear stresses. These stresses are called St. Venant stress τ_{st}, and the torque required to twist all of the plates in this way is the St. Venant torque M_{st}. (Murray, 1986, p. 8-9.)

To understand the meaning of a bimoment a small element dz of a beam is shown in figure 3, where bimoment M_ω is acting on its left end. It is illustrated by a pair of moments M that are separated by a distance e so

$$M_\omega = Me \tag{3}$$

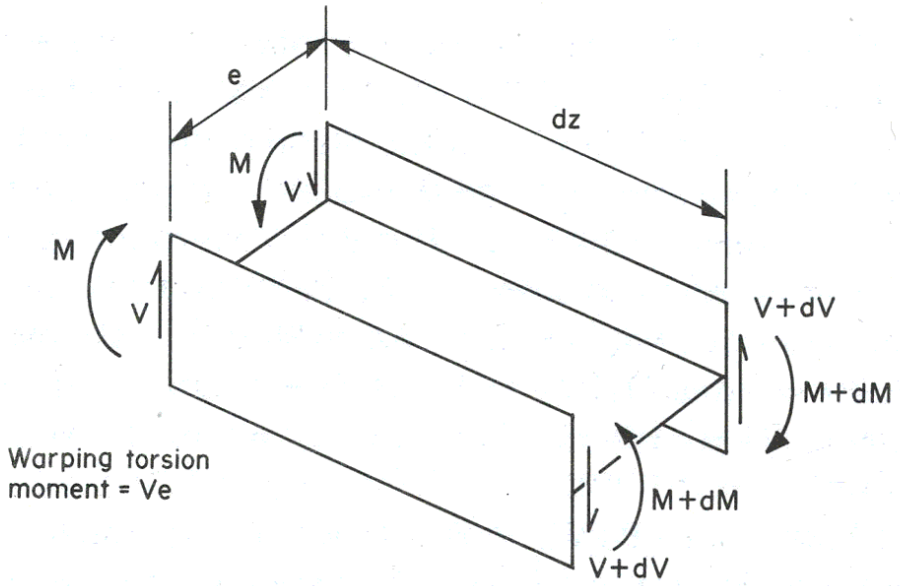

Figure 3. Bimoment in the small element dz of a beam (Murray, 1986, p. 9).

At the right end of the element the bimoment and the moment is assumed to have changed, so the bimoment on the right end is

$$M_\omega + \partial M_\omega = Me + e\,\partial M \tag{4}$$

In order to maintain rotational equilibrium in the flanges a transverse shear force V should exist in each flange, because it is assumed that the web is flexible out of its plane and cannot resist a force out of its plane. Thus

$$V\,\partial z = \partial M \tag{5}$$

So the shear forces form a pair at each end and this pair of forces is a warping torsion moment M_{DS}. When equations (3) and (5) are combined with the warping torsion moment equation, one can get:

$$M_{DS} = Ve = \frac{\partial M}{\partial z} e = \frac{\partial (Me)}{\partial z} = \frac{\partial M_{\omega}}{\partial z} \tag{6}$$

Otherwise the warping torsion moment is derivative of the bimoment with respect to the longitudinal coordinate z of a beam. A twisting moment appears when the bimoment varies along the length of the beam. There are shear stresses related to the force V. These stresses affect in the plane of the cross-section and are the warping shear stresses τ_{ω}. Furthermore, the moment M causes the direct warping stresses σ_{ω} to arise. (Murray, 1986, p. 9-10.)

2.3 Distortional forces

External loads affecting the walls of, for example, a rectangular cross-section can be divided into symmetric and antimetric load systems. Thereafter, the antimetric load system can be subdivided into pure torsional and distortional load systems. Division of the load systems is illustrated in figure 4. Any transversal load, which is not directed to the shear center of a cross-section, forms three subsystems and every subsystem causes mainly individual stress cases. (Kähönen & Niemi, 1986, p. 2.)

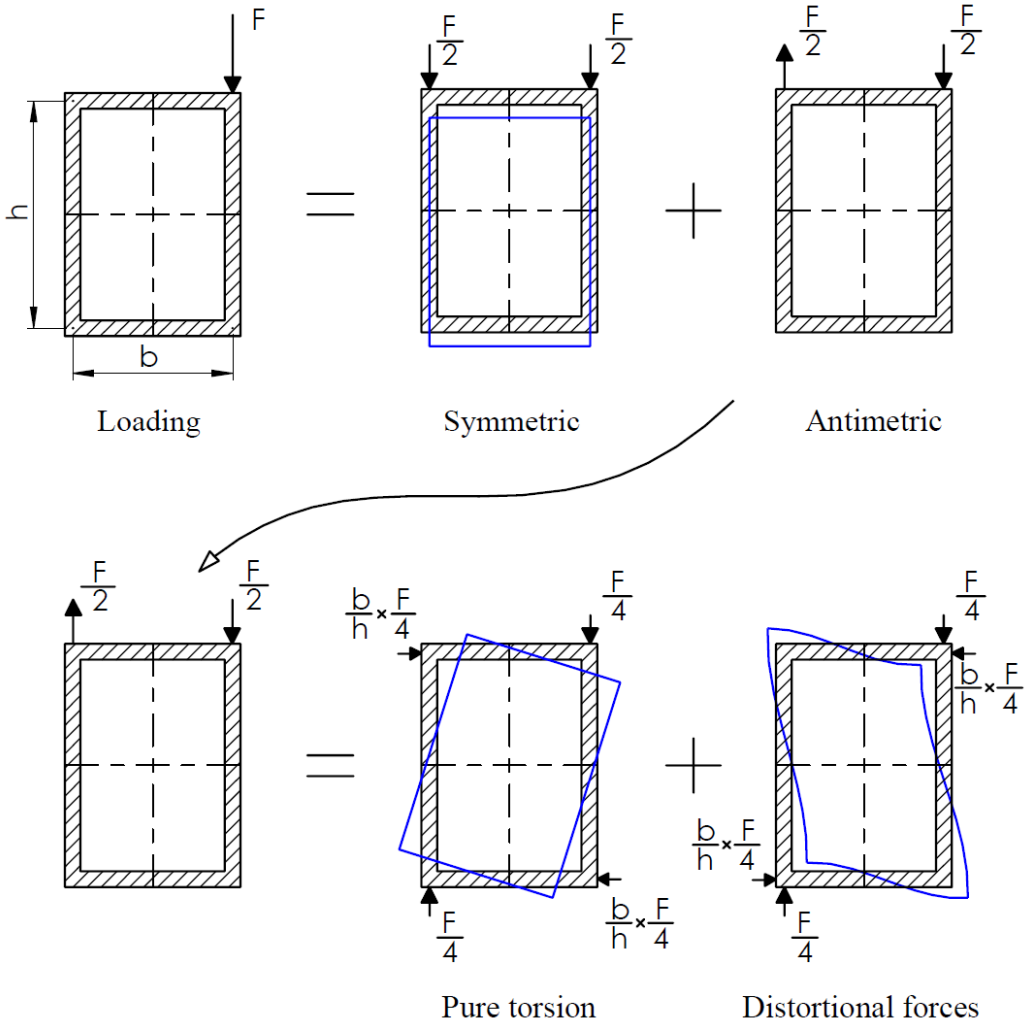

Figure 4. Division of an external load on the rectangular cross-section (Kähönen & Niemi, 1986, p. 2, modified by author).

Twisting moment does not exist in the distortion force system, because the external twisting moment is included in the pure torsion force system. The distortion forces can be divided into two sets of balanced loads, flange load F_f and web load F_w. Thus

$$F_f = \frac{b}{h} \cdot \frac{F}{4} \tag{7}$$

$$F_w = \frac{F}{4} \tag{8}$$

More detailed consideration of the deformations due to the distortional forces can be found in the report published by Niemi and Kähönen. (Kähönen & Niemi, 1986, p. 4.)

2.4 Primary shear stresses

The shear stress $\tau_{st,closed}$ in the closed profile caused by the pure torsion can be calculated with Bredt-formula: (Kähönen & Niemi, 1986, p. 2.)

$$\tau_{st,closed} = \frac{T_t}{2A_0 t} \tag{9}$$

In this equation (9) T_t is a torque in an arbitrary tubular member, in which A_0 is the area enclosed by the center line of its cross-section and t is thickness of the wall of the tubular member. It is possible to use this equation to calculate the shear stresses in closed profiles if the thickness of the wall is small, variations in thickness are not sudden and a cross-section has not re-entrant corners. (Timoshenko, 1956, p. 248.)

The shear stress $\tau_{st,open}$ for the open profiles that consist of the rectangular plates is defined as

$$\tau_{st,open} = \frac{T_t \, t_{max}}{I_t} \tag{10}$$

where t_{max} is the thickness of the thickest plate of the profile and I_t is torsional constant for non-circular shaft. (Pennala, 1994, p. 214.)

2.5 Warping stresses

The secondary shear stress τ_ω arises due to the warping and is defined as

$$\tau_\omega = \frac{M_{DS}(z) \, S_\omega(s)}{I_\omega \, t(s)} \tag{11}$$

where $M_{DS}(z)$ is the distribution of above defined warping torsion moment along a beam, $S_\omega(s)$ is a sectorial static warping moment at the particular point s in the cross-section, I_ω

is the warping constant and $t(s)$ is the thickness at the considered sector. (Pennala, 1994, p. 332.) The above mentioned shear stresses are pictured in figure 5. The secondary shear stress arises in both cases, the open and closed profiles.

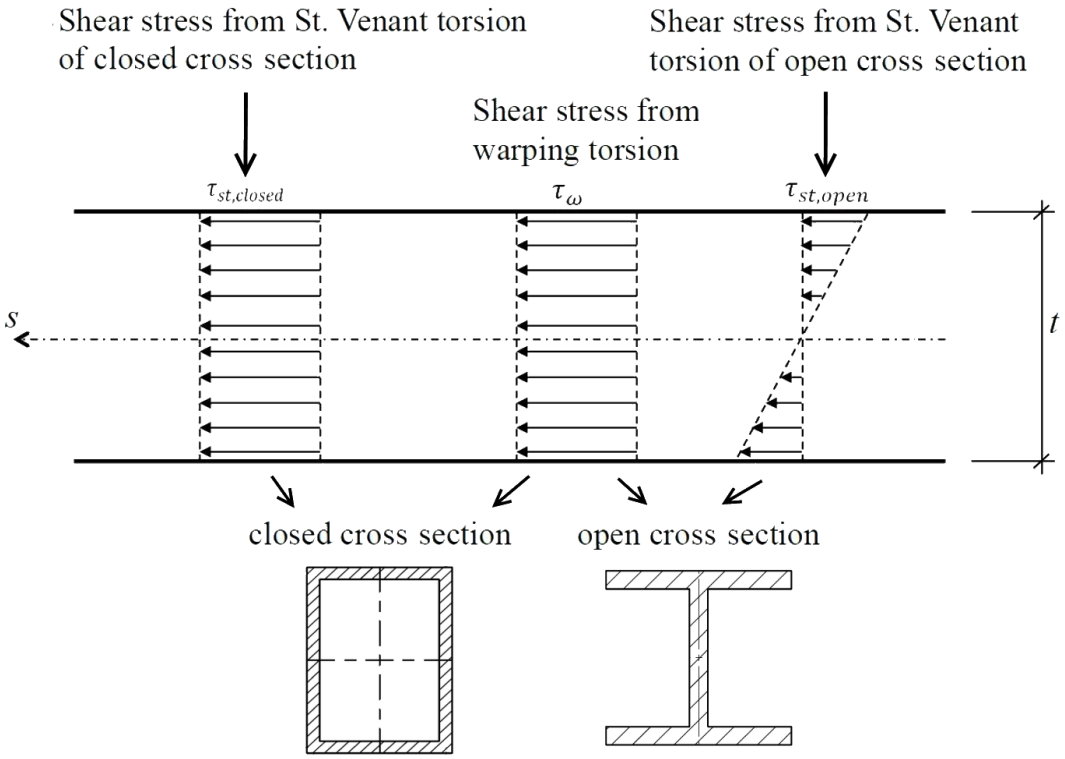

Figure 5. Shear stresses from St. Venant and warping torsion (Haukaas, 2014, p. 17, modified by author).

Longitudinal warping stresses σ_{ω} can be calculated using the last term of the equation (2):

$$\sigma_{\omega} = \frac{M_{\omega}(z)\omega(s)}{I_{\omega}} \tag{12}$$

where $M_{\omega}(z)$ is the distribution of the bimoment along a beam and $\omega(s)$ is the warping function. (Pennala, 1994, p. 332.)

Both torsion and distortion loadings cause warping stresses in the most rectangular cross-sections, but the first mentioned are insignificant when compared with the warping stresses due to the distortion loading. The distortion loading causes distortion stress in the transversal direction which is result from transverse bending of each plate of a rectangular cross-section

due to the distortional deformations. The distortion stresses can arise very high if the cross-section is not braced with diaphragms near the loaded cross-section. The diaphragms also reduce the warping stresses due to the distortion loading. (Kähönen & Niemi, 1986, p. 2.)

2.5.1 Warping constant of a single-cell closed section

Shear deformations have to be taken into account when deriving the warping constant I_ω of profiles with the closed cross-section. First the warping function $\omega(s)$ has to be defined. It is sectorial coordinate with respect to the shear center,

$$\omega(s) = \omega_0 - \oint_s \left(r_t - \frac{2A_0}{t \oint \frac{ds}{t}} \right) ds \tag{13}$$

where ω_0 is value of the sectorial coordinate at the starting point, r_t is a length of the normal from the shear center to the reference sector of the plate element. A_0 is the area enclosed by the profile, t is the wall thickness and s is the distance measured around the profile. (Björk, 2014)

$$I_\omega = \int_A \omega^2 \, dA = \oint_s \left[\oint_s \left(r_t - \frac{2A_0}{t \oint \frac{ds}{t}} \right) ds \right]^2 t \, ds \tag{14}$$

(Björk, 2014)

2.6 Secondary warping

Some thin-walled members have zero warping rigidity EI_ω, if calculated using the theory of thin-walled open sections. These sections are built from one or more rectangular elements which move away from a common point. Any warping shears in the mid-surface planes of those elements are concurrent, so the warping torsion moment M_{DS} is zero because it is defined as

$$M_{DS} = -EI_\omega \frac{\partial^3 \phi}{\partial z^3} \tag{15}$$

where ϕ is twist rotation about the longitudinal axis z of a beam element. (Trahair, 1993, p. 304.)

According to the thin-walled theory, warping displacement is zero during the torsion of the beams of rectangular, angle, tee and cruciform section. Boundary conditions associated with warping cannot be invoked if the warping constant I_ω is zero. Thus, theoretical solutions for the twisting of the beam have flaws at the points of concentrated torque and at the fixed supports. There are theoretical undefined points in $\partial\phi/\partial z$ in the above-mentioned regions, where rapid change of the twist rotation along the beam element happens. (Trahair, 1993, p. 304.)

These flaws can be fixed by including the effect of secondary warping, also called thickness warping, which is neglected in the thin-walled theory. The secondary warping constant $I_{\omega s}$ can be defined using the displacement u of an element $\partial s\, t$ of the rectangular element, which thickness is t. The element is illustrated in figure 6. (Trahair, 1993, p. 304-305.)

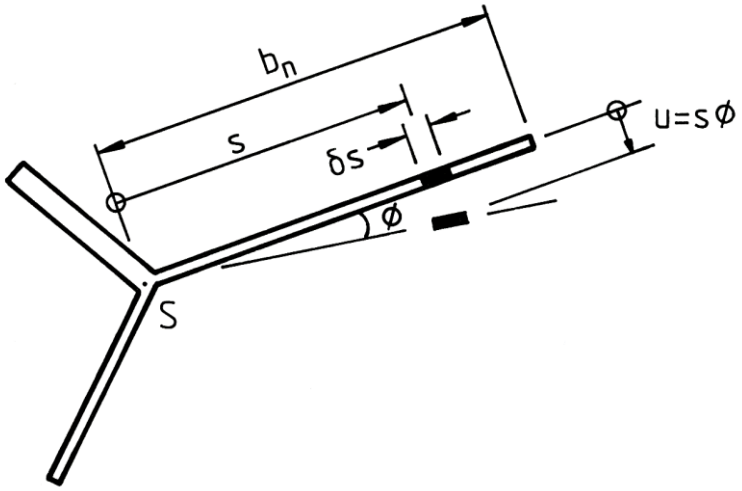

Figure 6. An arbitrary rotating section (Trahair, 1993, p. 305).

$$u = s\phi \tag{16}$$

As a consequence a shear component is developed due to the rotation. When the second moment of the area of the rectangular element is $\frac{\partial s\, t^3}{12}$, one can get

$$\partial V = E\frac{\partial s\, t^3}{12}u''' \tag{17}$$

Due to the shear component, a torque effect $s\delta V$ is developed, which acts about the axis of the twist through the point S seen in figure 6. The integrated effect of all such torque effects is equal to the secondary warping torsion moment M_{ws}.

$$M_{ws} = -EI_{\omega s}\frac{\partial^3 \phi}{\partial z^3} \tag{18}$$

where $I_{\omega s}$ is the secondary warping section constant. (Trahair, 1993, p. 305.)

The secondary warping section constant can be composed of equations (16), (17) and (18). Thus, the sum of the integrations over the area of every rectangular element in the cross-section gives

$$I_{\omega s} = \sum_n \int_0^{b_n} \frac{t^3 s^2}{12}\, ds \tag{19}$$

As a result

$$I_{\omega s} = \sum_n \frac{{b_n}^3 t^3}{36} \tag{20}$$

where b_n is the breadth and t is the thickness of the single element in the cross-section. (Trahair, 1993, p. 306.)

Double symmetric hollow rectangular sections act in the same way, but for different causes. The primary warping does not happen in such sections, because the warping deflections due to twisting are precisely balanced by the warping deflections due to the shear straining. (Trahair, 1993, p. 306.)

3 RESEARCH METHODS

A simple idea of the research issue is pictured in figure 7. The RHS beam is fixed at the left end and external torsion moment M_t affects at the right end of the beam. Material properties for steel are used in the FEA according to SFS-EN 1993-1-1:2005. Length of the beam is 500 mm or 1000 mm, depending on the loading and support variations. The reason for different lengths is calculation limit when using very fine mesh in FE-analyses. In these cases the torsion is set so that twist rotation along the axis z (figure 7) is the same for a more practical comparison.

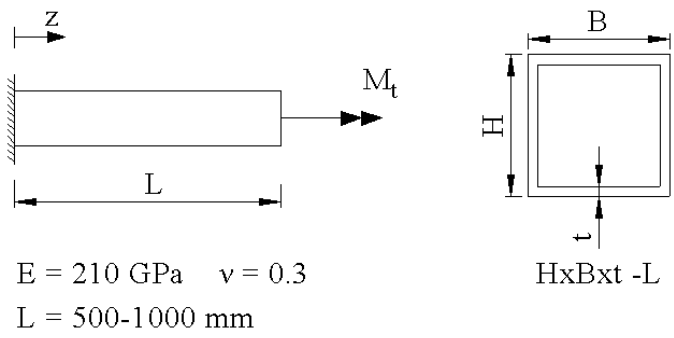

Figure 7. Principle of the structure of the models.

Every torsion case is analyzed by FE-method using mostly linear 8-noded solid and 4-noded plate elements. 10-noded tetra elements are used at the irrelevant locations in the very fine meshed solid models, where relevant locations are modeled with fine mesh using linear solid elements.

3.1 Load end variations

Torsional loading is set by two opposite shear forces so that bimoment comes across two bracket plates which are simply bending beams continuous from the webs of the RHS beam. The end diaphragm is placed after the bracket plates and the distance of the second diaphragm is varied in relation to the end diaphragm. One of the models can be seen in figure 8. Thickness of the diaphragms is same as the thickness of the RHS profile. In this structure the distribution and restraining of the distortion and primary warping is researched.

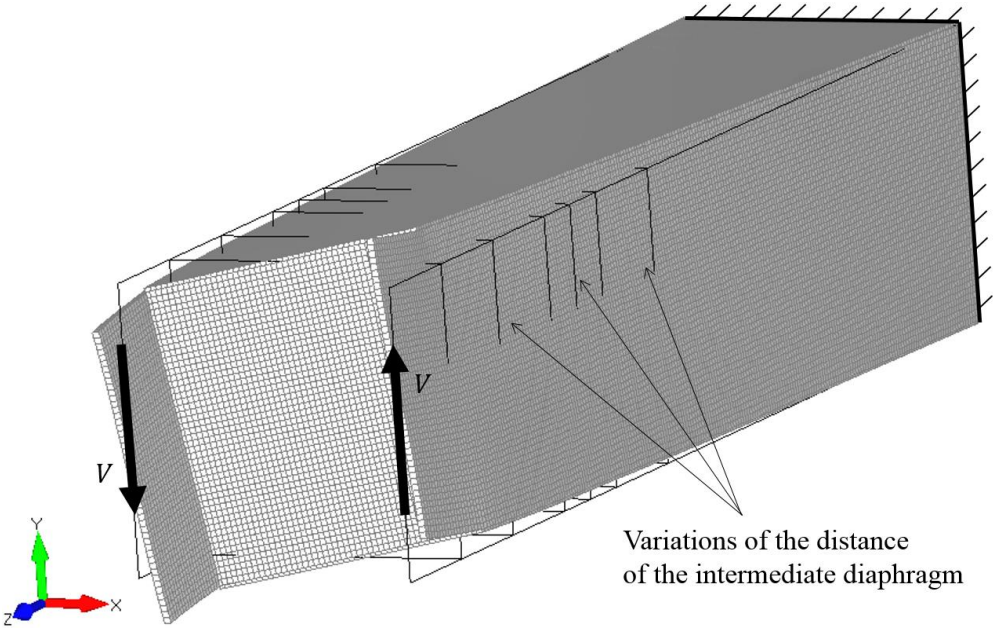

Figure 8. Plate element model of the torsion beam with the transverse shear forces V.

The second variation is pure torsion loading. This loading is set so that every flange and web has shear force that causes same amount of torsion on the beam. These force vectors are illustrated in figure 4, for example every four shear force is the same value for square cross-section in the case of the pure torsion. The primary and secondary warping, especially at the fixed end of the beam, are the research targets in this case.

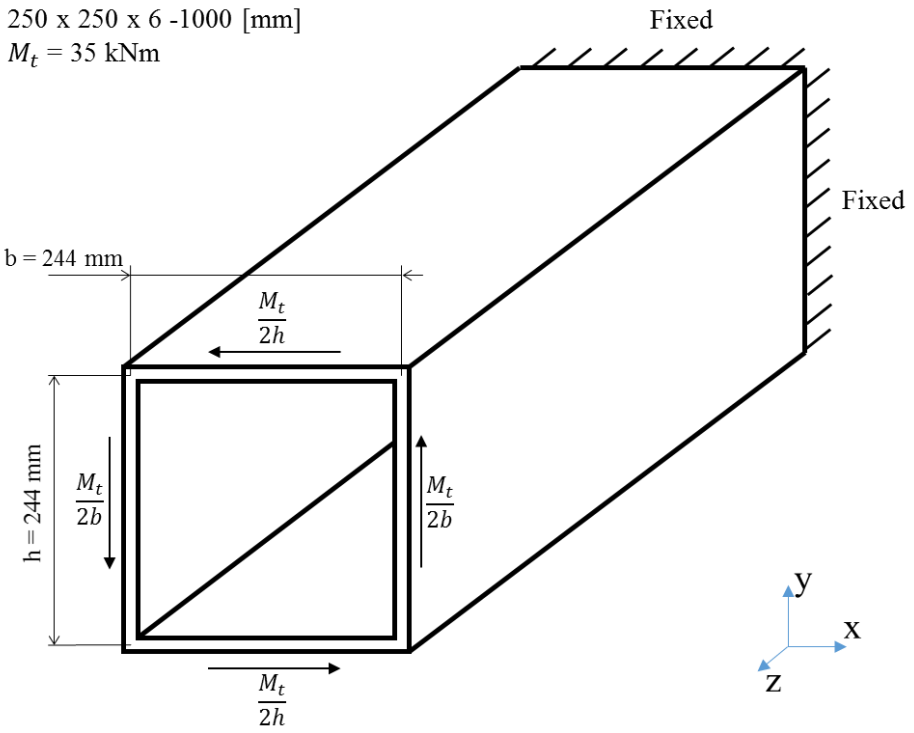

Figure 9. Pure torsion loading in the ideal square cross-section.

3.2 Support variations

In most of the analysis cases the support end is fully fixed, so that whole surface of the end cross-section is restricted to deform to any direction and all rotations. In consequence the maximum primary and secondary warping stresses are located exactly at the fixed end. This resembles the situation where the beam is welded with a full penetration butt weld to the rigid base.

More complex support is made to depict the weld at the beam end. The models point out critical toe and root stresses by using ENS-approach, and describe which one of them is more critical. It is important to understand that the constraints of the support end are different depending on the weld, such as butt weld with groove without root face or fillet weld with some penetration or none.

3.2.1 Effective notch stress approach

Effective notch stress approach is a method to obtain the effective stress at the toe or root of a weld, assuming material behavior as linear-elastic. The actual shape of the weld at the toe or root is replaced by a fictitious notch radius to take account of the variation of the weld shape parameters and non-linear material behavior and to avoid arbitrary or infinite stress results at the notch root. (Hobbacher, 2013, p. 29.)

The stress reduction in a notch due to averaging the stress over a certain depth can alternatively be achieved by a fictitious enlargement of the notch radius at the weld toe or root, see figure 10. Radaj assumed a fictitious radius of 1 mm for structural steels and aluminium and magnesium alloys. This notch rounding may cause problems in thin-sheet materials, so a small-size notch approach which uses a reference radius 0.05 mm has been proposed in this case. (Fricke, 2013, p. 763.)

Effective notch stresses are taken from the predetermined diagrams, or calculated by parametric formulae, finite element or boundary element models. For FE-analyses recommended element sizes are not more than 1/6 of the notch radius in case of linear elements, and 1/4 of the radius in case of higher order elements. (Hobbacher, 2013, p. 30.)

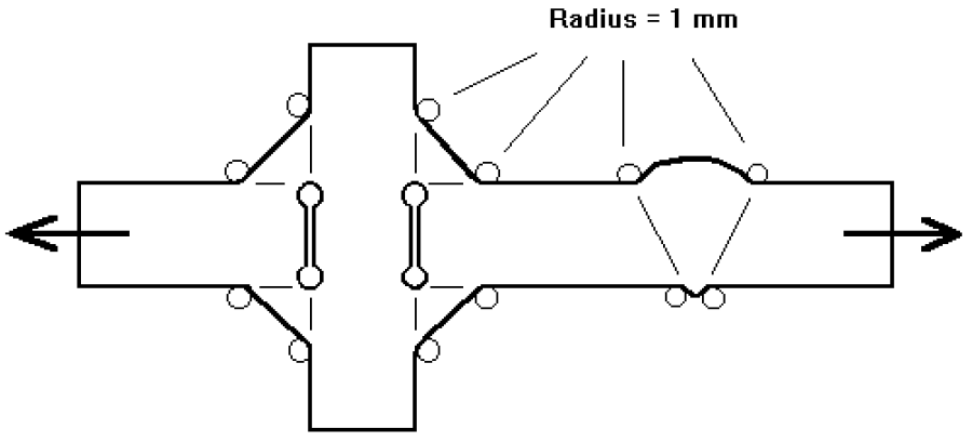

Figure 10. Example of the fictitious rounding at the weld toes and roots (Hobbacher, 2013, p. 30.)

The element model is analyzed with a rather rough mesh, which is locally refined near the notches under consideration. The mesh should be refined without large steps in element size and too much element distortion. (Fricke, 2013, p. 764.)

Compared to the nominal and structural stress approaches, the advantage of the effective notch approach is that the local stress in the weld root or toe is explicitly taken into account so that influencing geometrical and local stress distribution factors are considered. The weld geometry still has to be idealized, so example irregularities and residual stresses can only be considered by the chosen SN-curve. (Fricke, 2013, p. 763.)

3.3 Rubin's theory about torsion of structural hollow sections

This theory takes the rounded corner of the cross-section into account in the defining of the warping constant. An idealized square cross-section has a zero primary warping constant as stated early, but the primary warping constant differs, if the hollow section profile has the rounding at the corners. (Rubin, 2007)

Rubin studies hollow rectangular profiles according to EN 10210-2 and EN 10219-2. In his work the calculation of normal and shear stresses due to primary warping are clarified. (Rubin, 2007, p. 21.)

The secondary torsion constant I_{ts} is calculated to separate the magnitude of the secondary torsional moment from the total torsional moment:

$$I_{ts} = \frac{{I_\omega}^s t}{\int_0^U {S_\omega}^2 \, ds} \tag{21}$$

where $\int_0^U {S_\omega}^2 \, ds$ is the integration of the sectorial static moment over the whole center line of the tubular cross-section. (Rubin, 2007, p. 25.)

The secondary torsional moment M_{DS} is defined with a factor κ, thus

$$M_{DS} = \kappa M_t \tag{22}$$

where the κ is defined as

$$\kappa = \frac{1}{1 + \frac{I_t}{I_{ts}}} \tag{23}$$

(Rubin, 2005, p. 827).

The maximum bimoment M_ω at the fixed end can be calculated with a factor l_0, assuming that length of the beam L is much longer than height and breadth of the cross-section. (Rubin, 2007, p. 27.)

$$M_\omega = \kappa l_0 M_t \tag{24}$$

$$l_0 = \sqrt{\frac{E I_\omega}{\kappa G I_t}} \tag{25}$$

The normal and shear stresses of the warping torsion are now possible to calculate with equations (11) and (12). (Rubin, 2007, p. 28.)

4 RESULTS

The results of the element models are concerned in two separate sections. In the first section, the load end system where diaphragms are placed transversally to restrain the cross-sectional distortion and warping stress is examined. In the second section, the support end of the beam, such as warping stresses immediately after the support constraints and the effects of the weld at the support are studied.

4.1 The effect of the intermediate diaphragm on the distortion

The different structure cases were analyzed to clarify what distance of the second diaphragm was optimal by FE-method. Torsional loading was caused with pair of the brackets, which were continuous plates from webs of the beam, as is explained in chapter 3.1. The distortion in the beam with a square cross-section with different diaphragm setups is shown in figure 11. (Ahlfors, 2014, p. 1-20.)

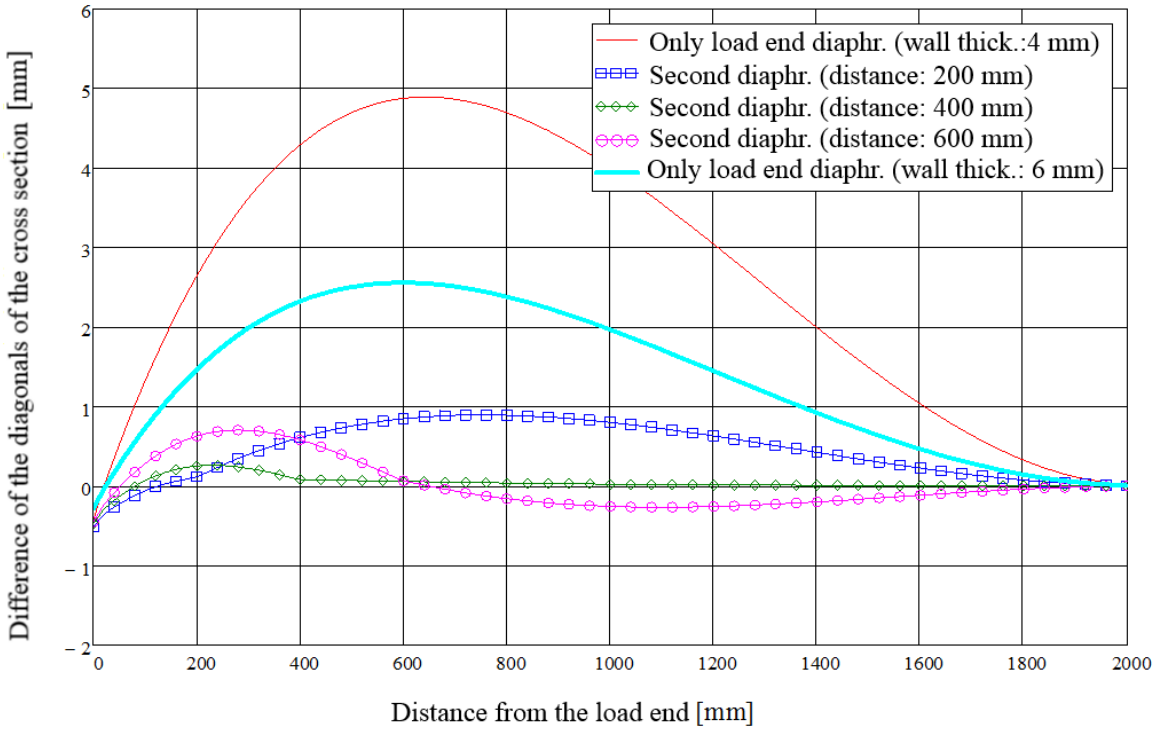

Figure 11. Distortion along the beam of square cross-section according to FE-analyses (Ahlfors, 2014, p. 15).

The distortional forces change when the breadth of the square profile is increased or decreased to get rectangular profile as figure 4 illustrates. Nevertheless, distortion along the beam behaves the same, as can be seen in figure 12.

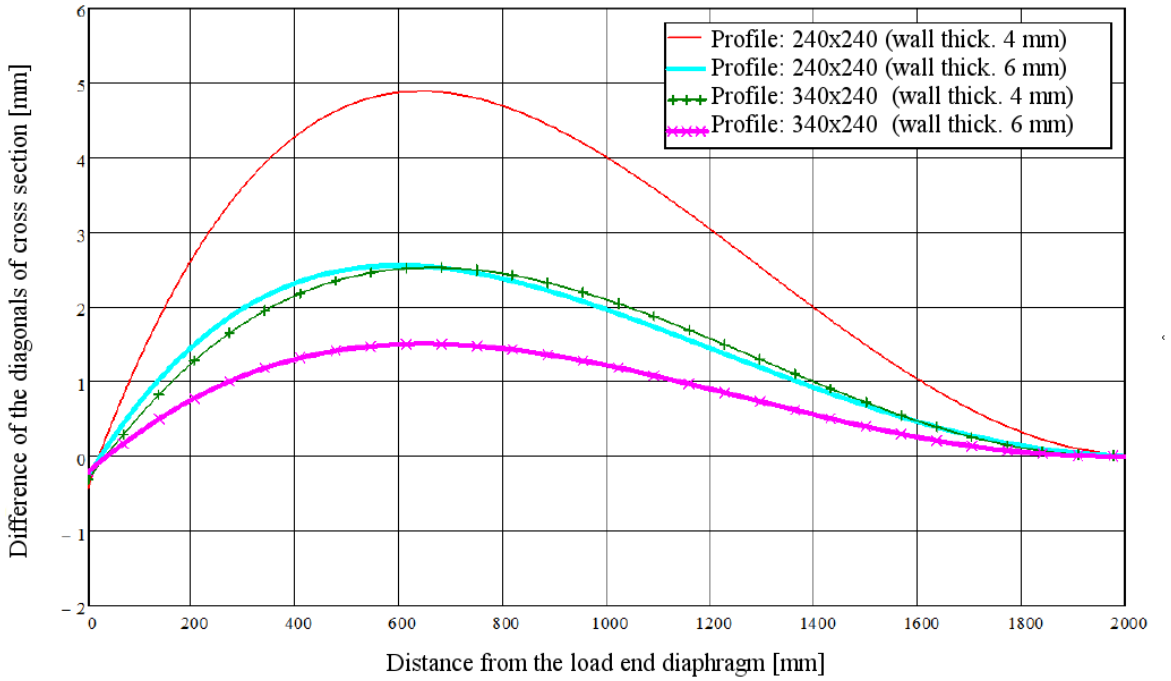

Figure 12. Distortion along the beam of square and rectangular cross-sections according to FE-analyses (Ahlfors, 2014, p. 16).

The restraining effect was also detected in the warping stresses. Increasing the wall thickness in the flanges and webs decreased maximum warping stress at the load end of the beam, but the double diaphragm structure restrained these stresses more effectively than a 50% increase in wall thickness, see figure 13. Figure 14 indicates behavior of the warping stress in rectangular cross-section with two different wall thicknesses with the diaphragm of the load end attached. The maximum warping normal stress is smaller compared to the square cross-section because of the difference in cross-sectional properties.

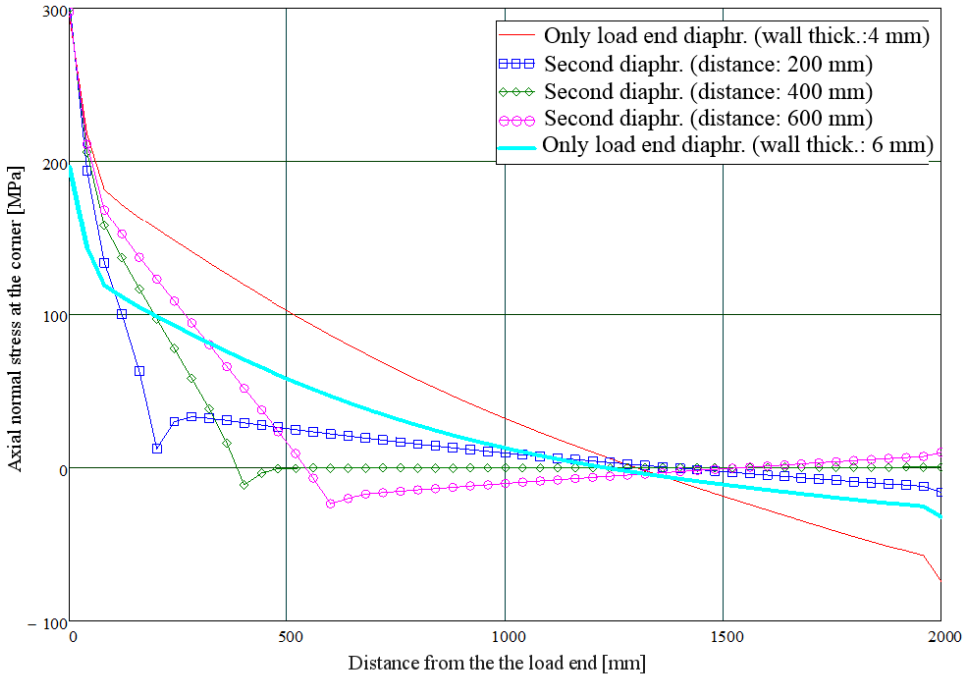

Figure 13. Axial normal stress at the corner along the square cross-section beam with the different diaphragm setups (Ahlfors, 2014, p. 17).

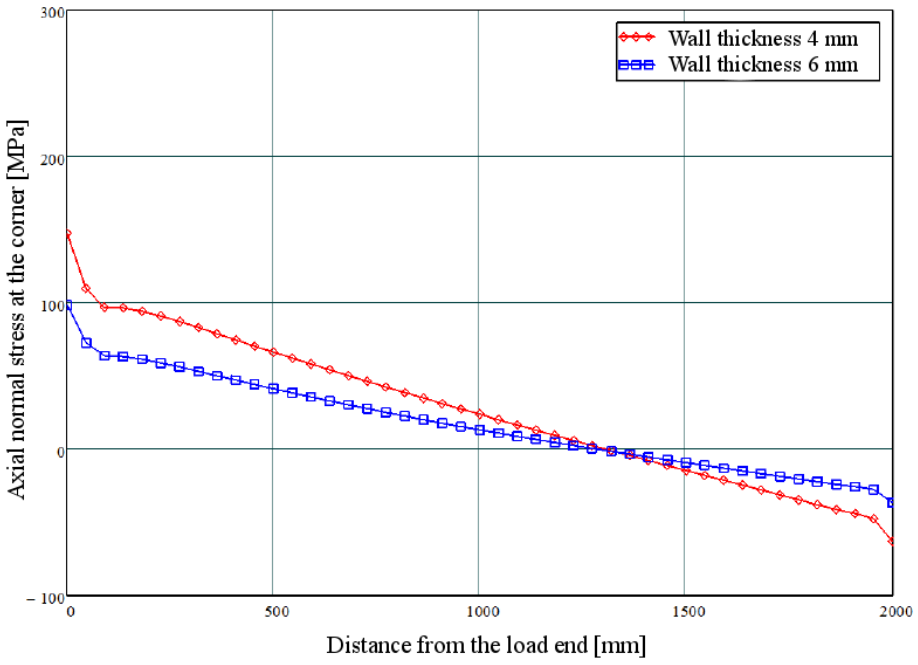

Figure 14. Axial normal stress at the corner along the rectangular cross-section beam (Ahlfors, 2014, p. 18).

The graph of figure 15 indicates the distortion of the different transverse diaphragm setups in the ideal square cross-section, so that difference of the diagonals of the cross-section are characterized along the torsion beam. A plate element model of the beam is loaded with the pair of shear forces at the end of the bracket plates, see figure 8.

The distortion is small in this beam, but more important is the restraining effect of the distortion with different variations and its resemblance to earlier research, as seen in figure 11.

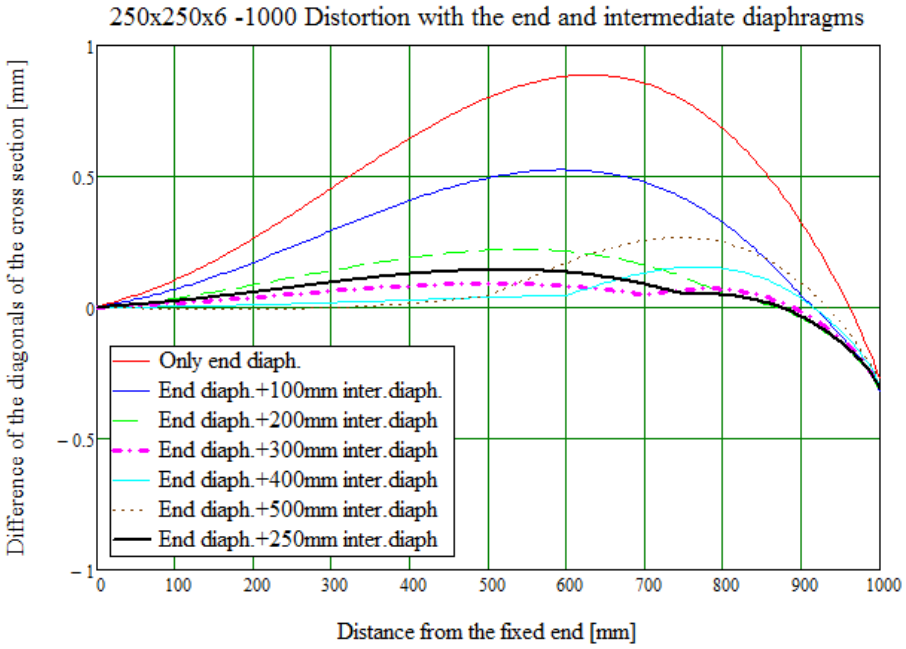

Figure 15. Distortion of the square cross-section with different diaphragm setups.

The next figure 16 shows the distortion of the RHS profile. The magnitude and load system of the torsional loading is the same as in the previous square section.

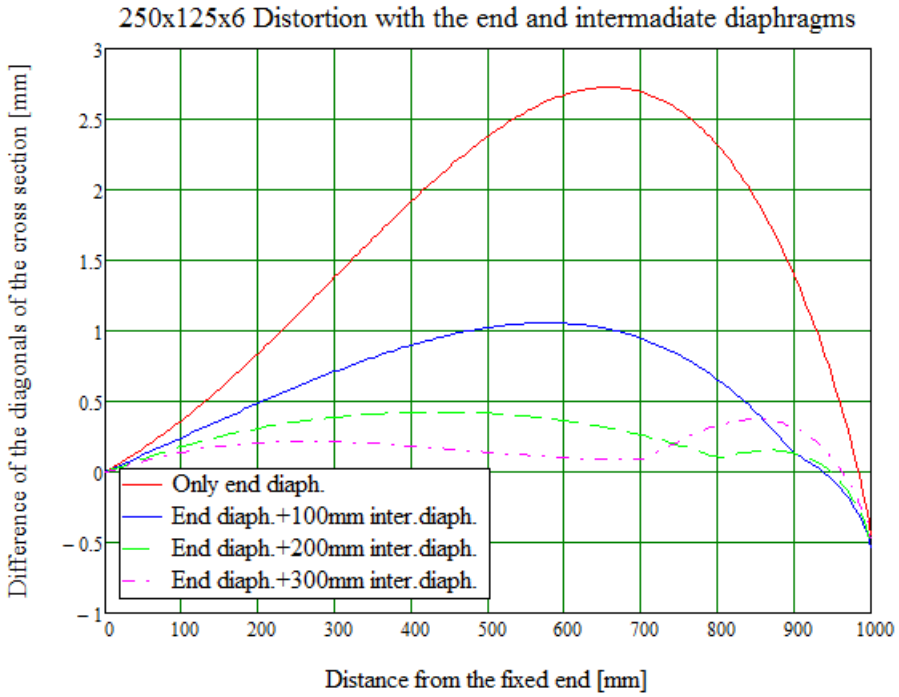

Figure 16. Distortion of the rectangular cross-section.

The graphs of the figures 17 and 18 indicate axial membrane stress at corner of the beam, in other words maximum primary warping stress. The figure 17 shows the results from SHS 250mm×250mm×6mm with seven different diaphragm positioning cases, and the figure 18 is from RHS beam with the cross-section dimensions 250mm×125mm×6mm. The fixed end is at the origin of the graph and bracket plates of the external load starts at right end in all these graphs (figures 15, 16, 17 and 18).

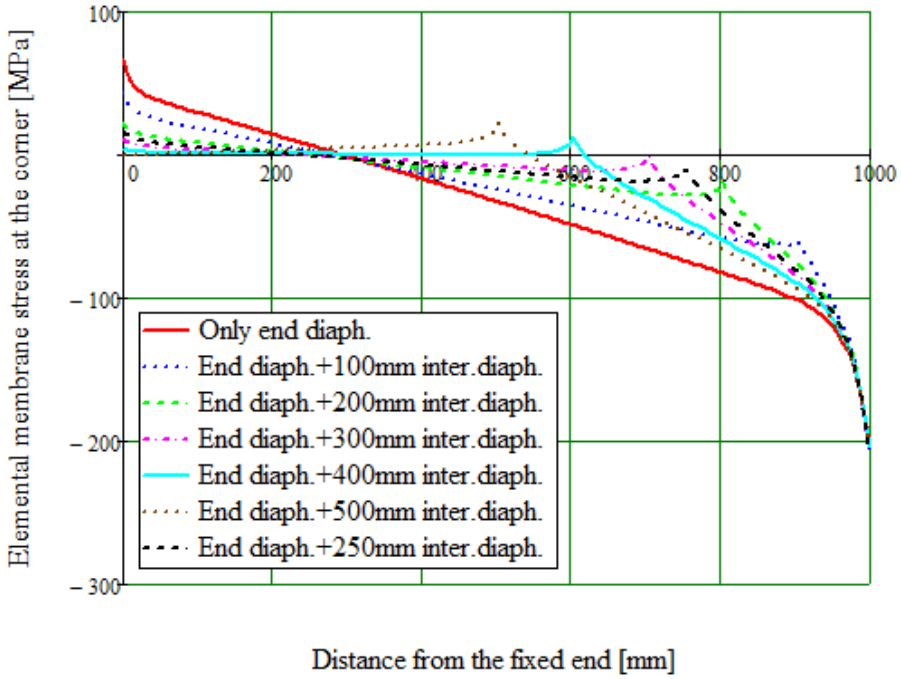

Figure 17. Maximum membrane stress along the beam with SHS profile.

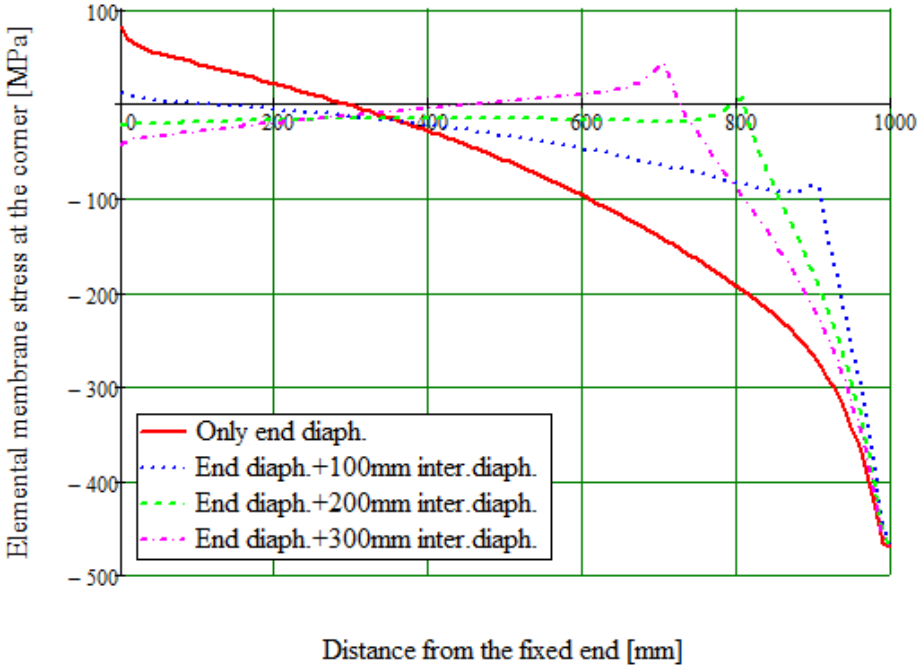

Figure 18. Maximum membrane stress along the beam with RHS profile.

4.2 Warping in the structural hollow section

This section contains the results from FE-analyses of structural hollow sections with square and rectangular sections under pure torsion loading. Dimensions of the structural hollow section models followed the requirements of the standard SFS-EN 10219-2. The primary

warping stress was determined from the center line of the wall thickness as shown the line segment *s* in figure 19 of the rectangular structural hollow section.

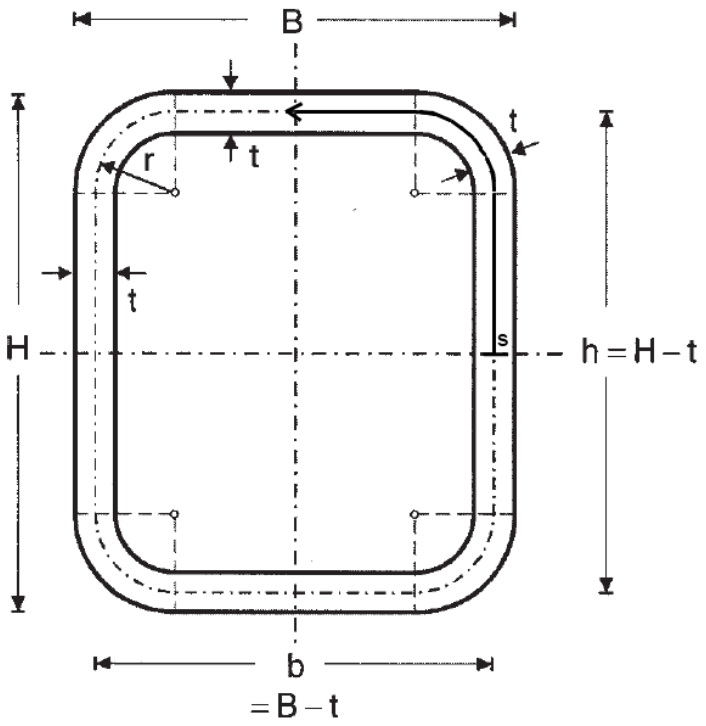

Figure 19. Rectangular structural hollow section (Rubin, 2007, p. 22, modified by author).

The dimensions of the two structural hollow sections were 150mm×150mm×8mm and 200mm×100mm×8mm, and the length of both beams were 500 mm. The beam was loaded with 9.5 kNm pure torsion, so that distortion did not occur and the change of rotation was linear along the beam. The model of the square section is shown in figure 20 with the axial stress contour on, in this case z-axis normal stress. Maximum axial stresses arises at the fixed end of the beam as the warping of whole plane of the cross-section is restrained.

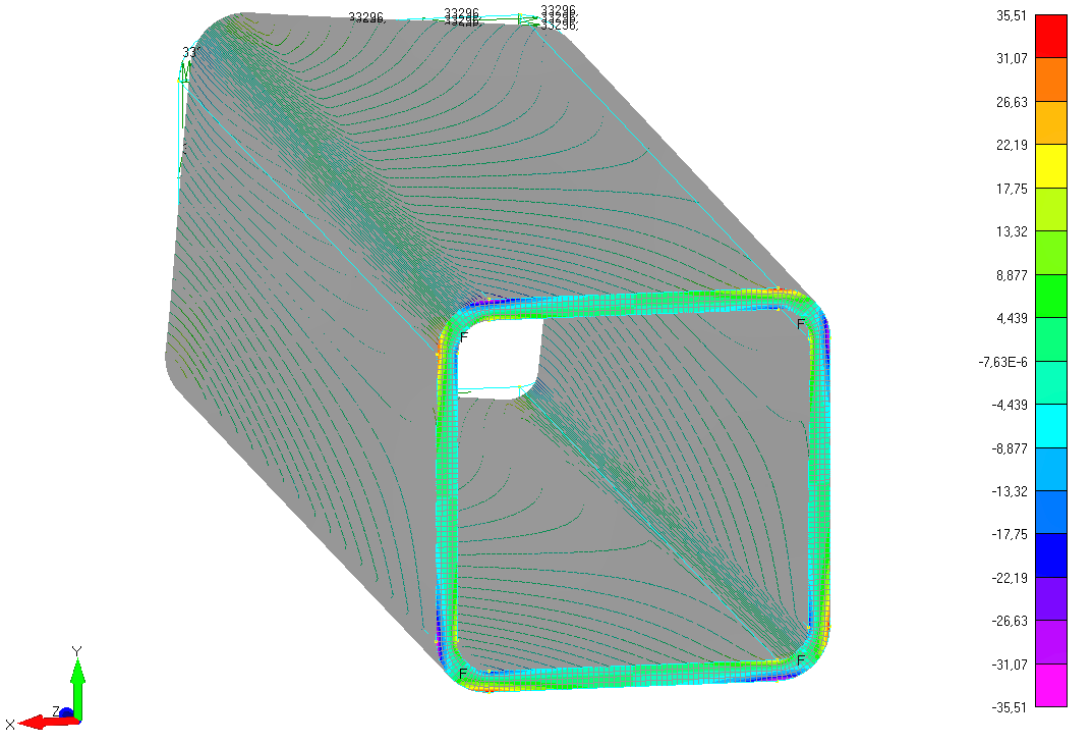

Figure 20. The model of the square structural hollow section with the axial stress contour on.

The same kind of behavior was also found with the ideal square cross-section. Its corner of the fixed end is shown in figure 21, where secondary warping causes maximum axial stress to arise at the corner on the top of the web and flange plates. The black lines in figure 21 indicates the line where axial stress is zero. Theoretically it should go along the center line of the cross-section, but the model of the figure 21 (250mm×250mm×6mm) and other models with different wall thicknesses and solid element sizes expressed that in addition to the secondary torsion of the flange and web, there was also a membrane stress affecting the system that resembled primary warping.

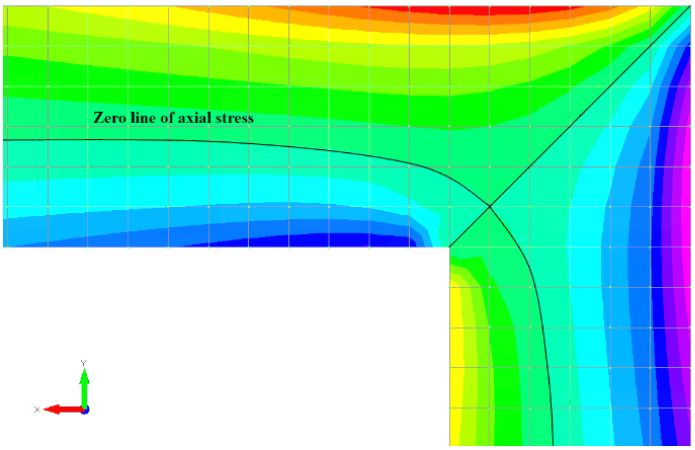

Figure 21. Axial normal stress contour at fixed corner of the ideal square cross-section.

The graph in figure 22 represents significant the axial stress effect is compared to primary shear stress, so called Bredt's shear stress. Stresses were taken as an average nodal stress from the corner of the fixed end to half way of the flange in figure 21. The membrane stress in the plate element analysis was negligible. In other words, the flanges and webs were only in bending stress state apart from Bredt's shear.

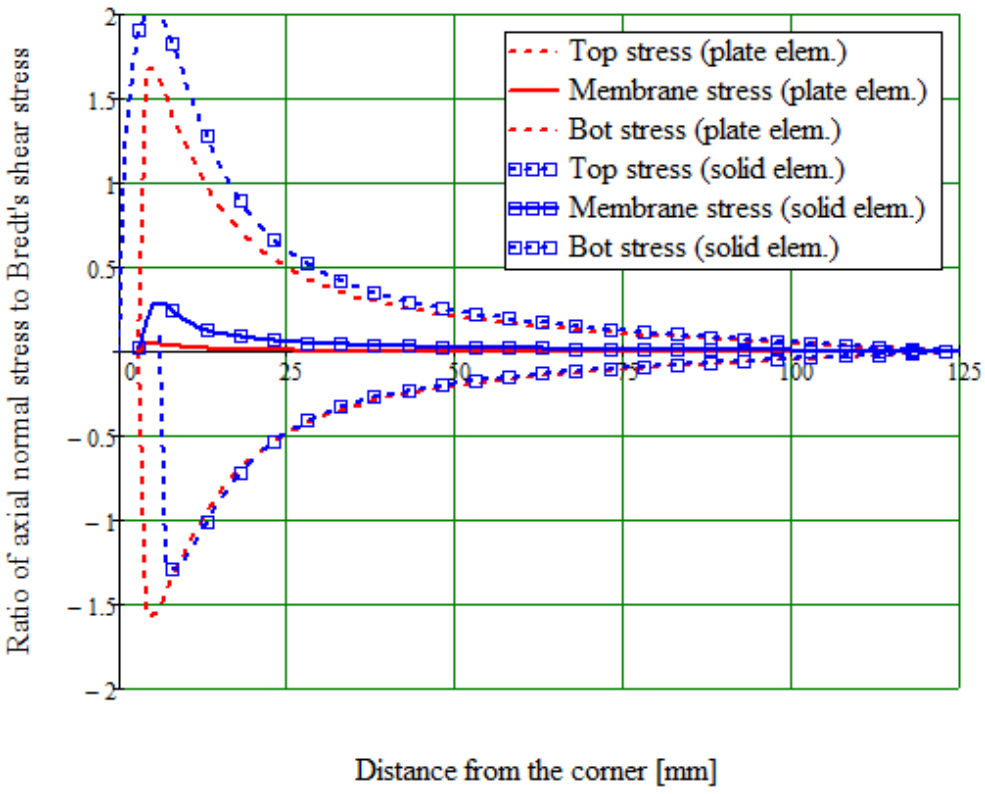

Figure 22. Axial stresses compared to Bredt's shear stress from the corner to half way of the flange in the ideal square hollow section in the plate and solid element models.

The primary warping in a structural hollow section was studied using the linear solid and plate element models. The dimensions of the cross-sections are shown in figure 23. The pure torsion caused primary shear stress is around 30 MPa. The magnitude of the primary warping stress along the line segment *s* (figure 19) is represented by the graph in figure 24, the quarter of the square cross-section. Figure 25 indicates the same, but in the rectangular cross-section. The primary warping stress is considerably higher in the rectangular cross-section than in the square cross-section.

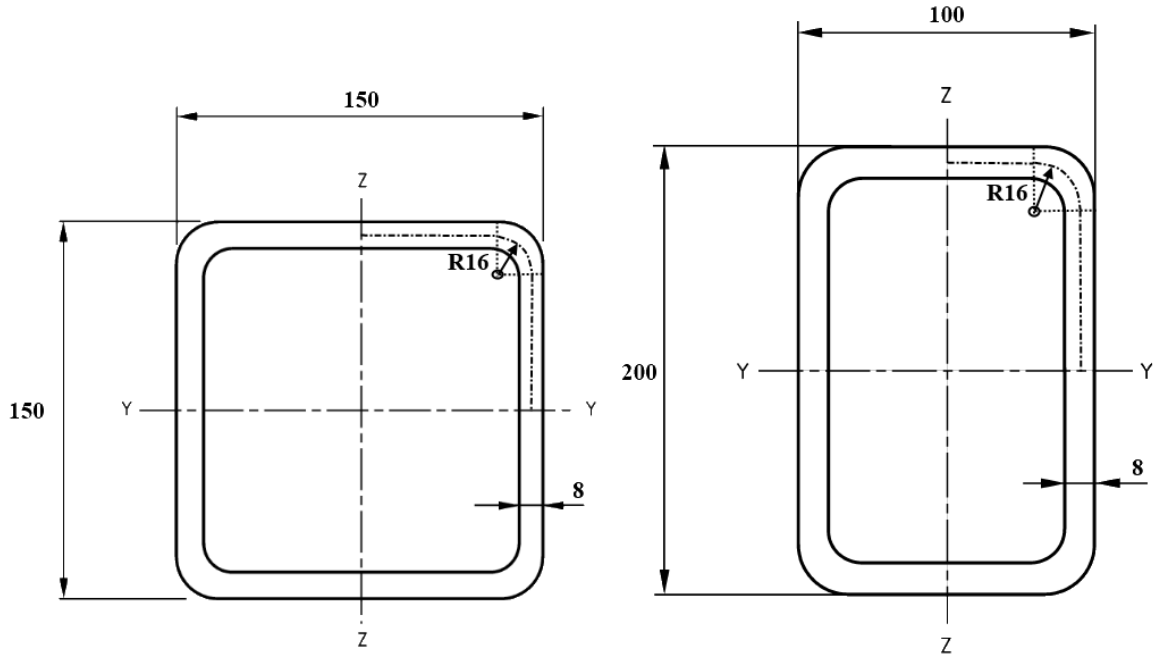

Figure 23. Dimensions of the models of structural hollow sections.

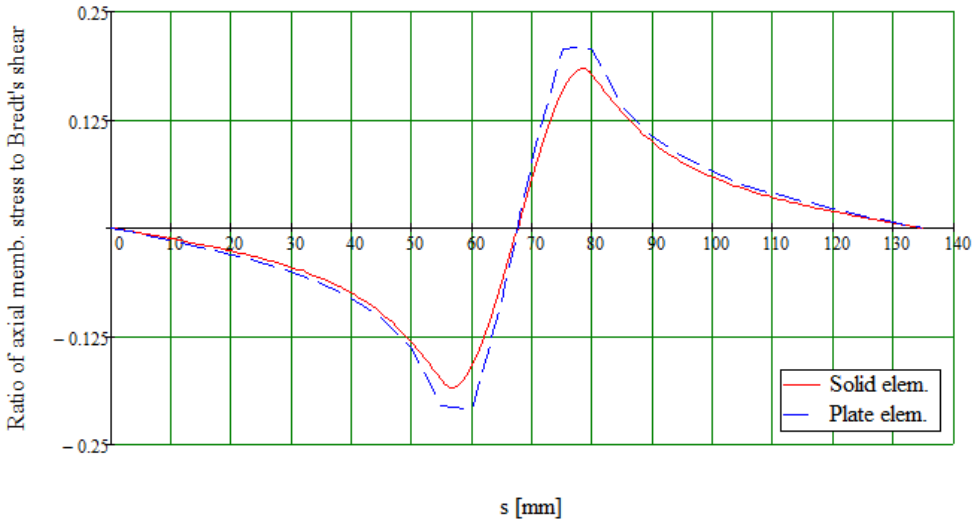

Figure 24. Primary warping stress along the line segment *s* in the quarter of the square structural hollow section, analyzed with solid and plate element models.

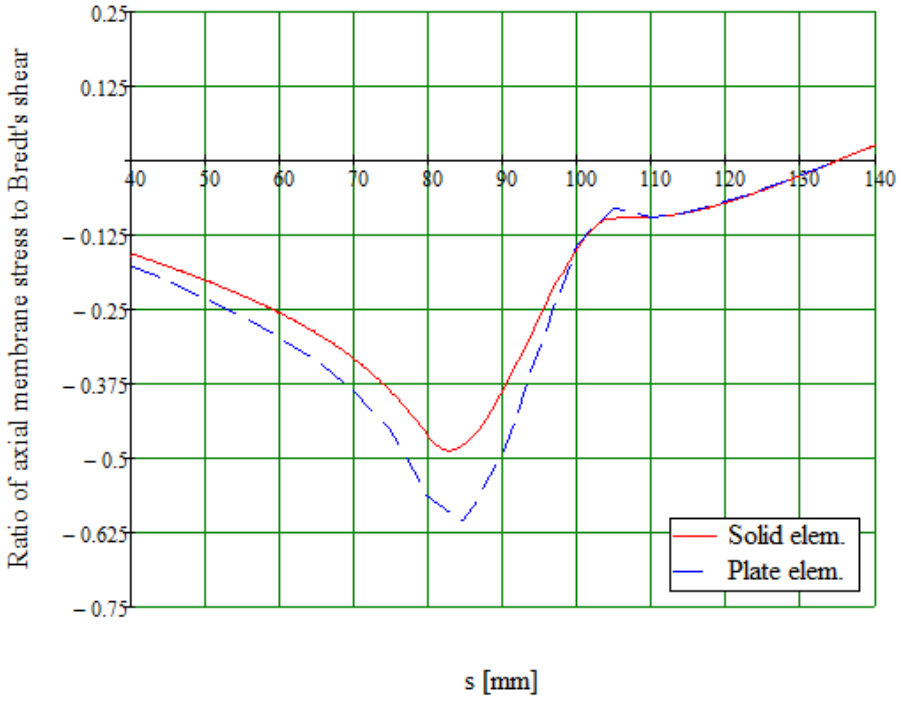

Figure 25. Primary warping stress along the line segment s in the rectangular structural hollow section, analyzed with solid and plate element models.

4.3 Results from the effective notch stress approach

Three different welds were modeled at the end of the beam, which was only a fixed surface in previous models. As stated before, 1 mm fictitious notch radius was selected, as shown a fillet weld with half penetration of the wall thickness in figure 26. Other modeled welds were a single bevel weld and a fillet weld with non-penetration. The effective throat was $1.1t$ in the fillet welds.

The dimensions of the analyzed models were same as in the previous section, see figure 23. Fine mesh (mesh size 0.1-0.2 mm around fictitious notch) was used in the neighborhood of the notches under consideration with the linear 8-noded solid elements. Sector cut of the square structure hollow section is shown in figure 26, where maximum principle stress contour is on. In all cases the critical notch was the toe notch.

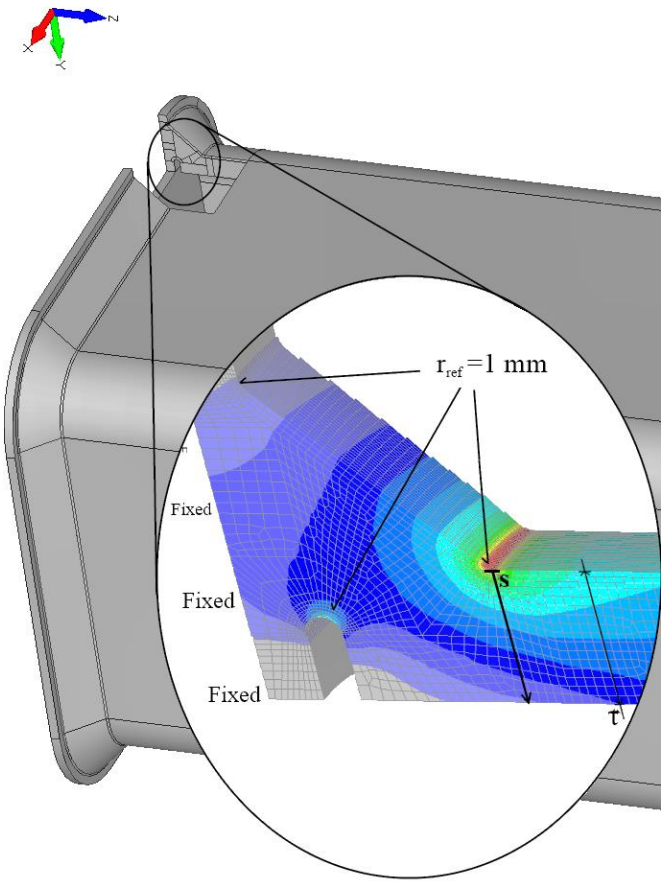

Figure 26. Element model with the fictitious notch rounding.

Stress distribution through the wall thickness of the square cross-section is shown in figure 27. The axial normal stress, primary shear stress and maximum principle stress are shown in the graphs, where s indicates the distance from the weld toe. The graph of figure 27(a) shows the stress distributions in the single bevel weld, 27(b) is the fillet weld with half penetration and 27(c) is the non-penetrated fillet weld. The graphs indicate that fillet welds with the half penetration and non-penetration do not differ much from each other. Furthermore, the least critical of these three cases is the single bevel weld.

The same torsional load causes nearly the same primary shear stress to the earlier mentioned rectangular structural hollow section (200mm×100mm×8mm). Stress distribution through the wall thickness with this profile is shown in figure 28. The single bevel weld is in the graph in figure 28(a) and the fillet weld with non-penetration is in figure 28(b).

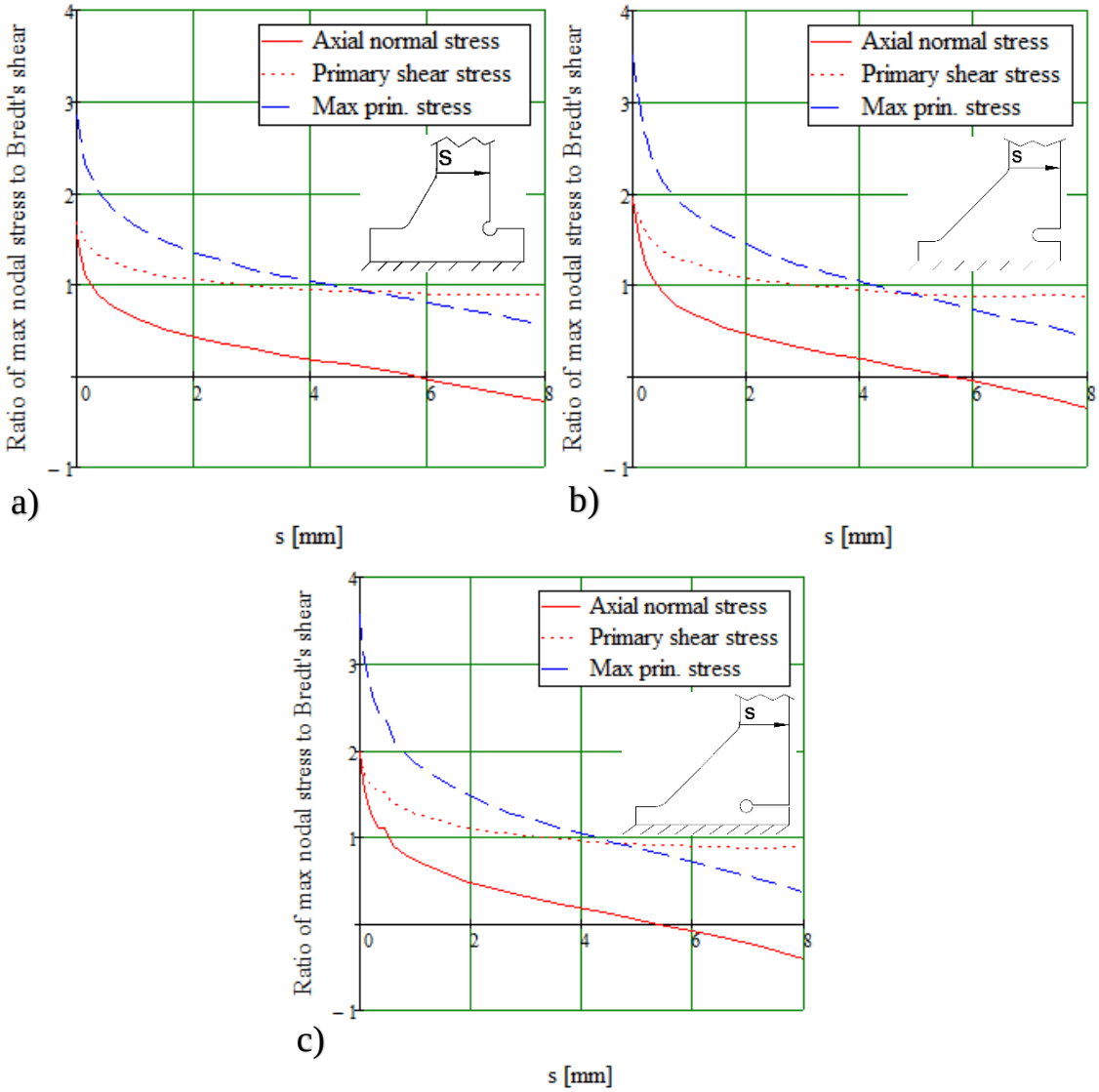

Figure 27. Stress distribution through the wall thickness in the square cross-section.

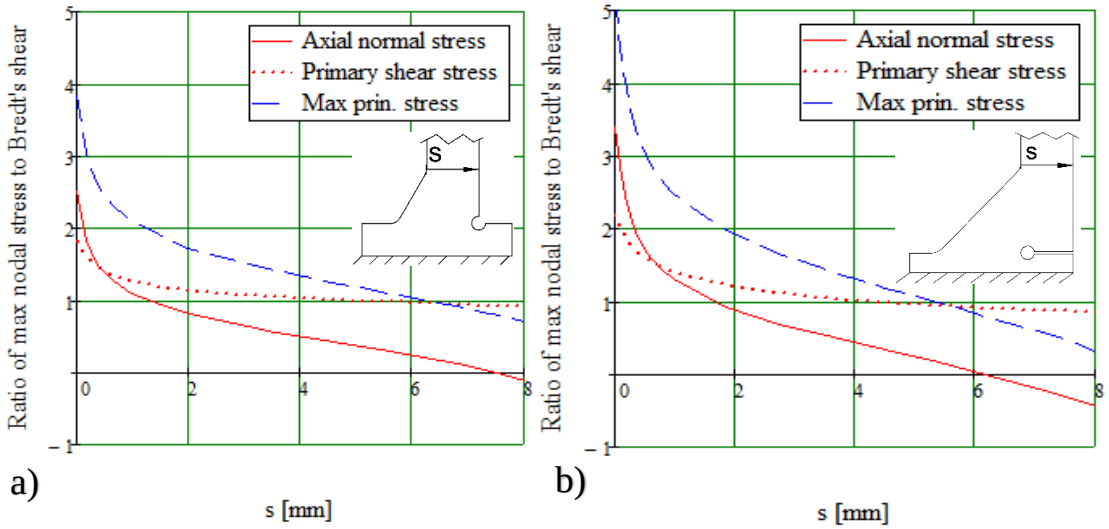

Figure 28. Stress distribution through the wall thickness in the rectangular cross-section.

4.4 Rubin's analytical method for primary warping

Distribution and maximum value of the primary warping in the structural hollow sections is also possible to calculate by Rubin's analytical method. The method is based on the accurate evaluation of the cross-section properties with constant wall thickness and dividing the torsional moment into the primary and secondary torsional moments.

Table 1. Warping and shear stresses relation to the Bredt's shear stress in the structural hollow section by FEA and Rubin's method.

	Rubin's method	FEA, solid elem.	FEA, plate elem.
Max. primary warping stress σ_ω/τ_{st}			
150x150x8	0.17	0.18	0.21
200x100x8	0.94	0.49	0.61
Primary shear stress τ_p/τ_{st}			
150x150x8	Uses Bredt's shear stress	0.94	0.98
200x100x8		1.02	1.07
Max. secondary shear stress τ_ω/τ_{st}			
150x150x8	0.12		
200x100x8	0.33		

More detailed calculations of Rubin's method is presented in appendix I, where the cross-section properties of the square structural hollow section (150mm×150mm×8mm) are evaluated by Rubin's method, which is presented in his publication Torsions-Querschnittswerte für rechteckige Hohlprofile nach EN 10210-2:2006 und EN 10219-2:2006.

The last mentioned structural hollow sections were also examined with AGIFAP (Advanced Graphical Interactive Frame Analysis Package). AGIFAP has been developed by the department of mechanical engineering of Lappeenranta University of Technology. It is an advanced 3D frame analysis element based tool, which was used in this study to verify the warping function ω of the studied structural hollow sections. The warping function of the square and rectangular hollow sections by AGIFAP is shown in appendix II.

5 DISCUSSION

The results showed that the second transverse diaphragm had a significant effect on restraining the distortion compared to the commonly used only end diaphragm. The second diaphragm was placed at a distance of $0.3L$ (and compared to the height of the beam: $1.2H$), the absolute value of 300 mm, from the end diaphragm in the best distortion restraining structure, which means that according to this thesis the distance has to be more than the height of the square cross-section. Nevertheless, this distance should not be too much or else distortion will occur between the first and second diaphragms.

Rectangular cross-sections distort significantly more than square cross-section with the same external loading, mostly because of the smaller height of the cross-section in this research. The best distortion restraint was achieved when the distance of the second diaphragm was around $0.2 - 0.3L$ (and $0.8 - 1.2H$) from the end diaphragm, thus the absolute value was around 200-300 mm.

The axial membrane stress, the primary warping stress, at the corner which arises due to the bending of the bracket plates can be restrained more effectively by an intermediate diaphragm. This decreases warping at the fixed end, since the bending stress of the bracket plates arises at the load end in any case. The primary warping stress was fully restrained when the second diaphragm was located $0.4L$ (and $1.6H$) from the first diaphragm and primary warping stress only had an effect between these diaphragms, as can be seen in figure 17.

The axial membrane stress behaves a little bit differently in rectangular hollow sections than in the last mentioned square hollow section, because primary warping also arises from the primary torsion, so axial stresses were higher in the rectangular section. The primary warping stress was near zero when the second diaphragm was at a distance of $0.2L$ (and $0.8H$). This means the primary warping and distortion were restrained a little bit by different setups of the diaphragms. However, a compromise between these diaphragm locations could restrain both warping and distortion effectively. The major problem is instead the manufacture of

this kind of structure as the welding should be done continuously around the second diaphragm inside the hollow section.

The initial target of this study was to determine the reason why ideal square cross-section appeared to behave like it had non-zero primary warping rigidity, because there was observed an axial membrane stress state similar to primary warping stress near the corners of the cross-section with solid element model analyses. However, this kind of behavior was observed only with solid elements and warping of the plate element models were only secondary. It was seen in figure 22 that the membrane stress at its highest compared to primary shear stress analyzed with plate elements was insignificant, while the membrane stress with solid elements was as much as 25 % from the primary shear stress.

A square section modeled with the plate elements represents differently the ideal square section than a solid element model. Plate elements form a continuous square where the flange and web connects with one axial node set, in comparison with solid elements that form in one sense the connection with thicker wall thickness at the corners. This affects the warping function in common with the rounding of the structural hollow section.

Distribution of the bimonent and so on the warping stress is also possible to calculate analytically by Khan and Tottenham method, but it is more suitable for open profiles. When the relation of the torsional constant to the warping constant (torsion characteristic, equation (1)) increases too much the method does not apply anymore and torsion is assumed to be merely uniform torsion. These calculations are not used in this paper for this reason. This might lead to a situation where the warping stresses are predicted too high.

Rubin's method is more suitable for more warping rigid cross-sections, though it is a slightly complicated way to derive the exact warping function. However, in cases with simple structures it is pointless to make fine meshed element analysis to solve the primary and secondary warping stresses.

Not only external dimensions and wall thickness define the warping constant of the structural hollow section. In addition, the corner radius has influence on the warping constant, as a matter of fact the corner radius is the reason for non-zero warping rigidity in square structural

hollow section. In the square section case, the influence depends on the radius in relation to the height of the cross-section. Studies showed that when the corner radius was around a sixth of the height of the cross-section the maximum value of warping function was the highest. Graph in figure 29 shows the behavior of the maximum warping function, which arises at the start of corner in the rounded square cross-section, when radius of the corner is changed. The warping function in figure 29 is derived from earlier mentioned Rubin's method and divided by quarter of the area enclosed by an acute-angled profile.

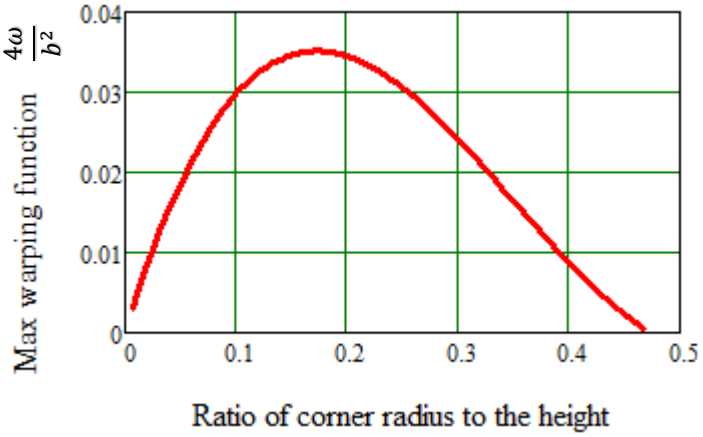

Figure 29. Influence of the ratio of the corner radius to the height of the cross-section on maximum warping function value relation to quarter of the area enclosed by an acute-angled profile.

The primary warping has a different constraint set than the secondary warping, otherwise the warping of the individual web or flange plate can roil the situation when membrane deformations are restricted and assumed to behave only as a primary system. For example, an under-dimensioned weld acts secondarily as a rigid constraint if the structure is rigid as for warping, such as square box girder, however it gets affected by the secondary warping stress.

5.1 Future research

Only transverse diaphragms axially perpendicular to the beam was studied. In the future research also diagonal diaphragms could be observed, in that case one diaphragm might have more effective area of the cross-section to restrain the bimoment and shear forces. Another case could be transverse circular or ellipse hollow section inside the hollow section beam at the load end. Different restraining systems shown in figure 30.

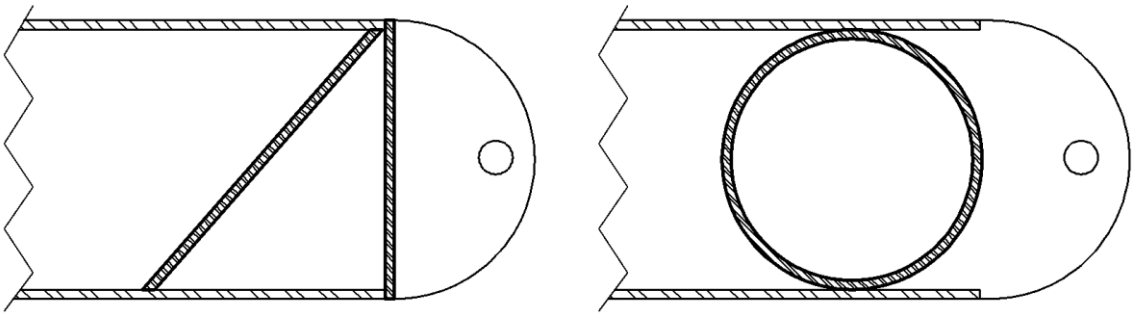

Figure 30. Some of the diaphragm assemblies for future research.

Kähönen and Niemi presents analytical method to solve the distortion by BEF (Beam on elastic foundation). Restraining of the distortion could be estimated with intermediate transverse diaphragms by this method. (Kähönen & Niemi, 1986, p. 11-16.) However, this method requires the understanding of the analogy of the beam on elastic foundation, and could be good point of comparison for the FE-analyses.

Analytically calculated primary warping stress in the rectangular cross-section was quite high by Rubin's method compared to the stresses obtained from the FE-method. Wider examination is necessary and more different cross-sections should be considered.

6 SUMMARY

The distortion and primary warping due to the non-uniform torsion can be restrained with multiple transverse diaphragms at the load end of the beam under the torsional loading more effectively than with one diaphragm. The problem is the attachment of the inner diaphragm in this case, so benefits must be measured and in some cases the thickening of the wall thickness could be a more profitable solution. Nevertheless, thin-walled structures are good application for high strength steel, because of their light weight, so other options, than increasing the wall thickness, should be considered.

The warping has no influence on the ultimate strength of the closed hollow section structures in the torsion loading, thus the primary and secondary warping stresses are assumed negligible in the most cases. However, these stresses should be taken into account, if the aim is the accurate prediction of the fatigue strength.

As long as the SHS has no ideal right corners it has not only secondary warping rigidity, but also primary warping rigidity. Hence, the axial membrane stress arises due to the external torsion loading in the square cross-section. The corner rounding also increases the warping of the rectangular cross-section compared to the ideal corners. This effect is small, but can explain some fractures and initial crack points.

REFERENCES

Ahlfors, M. 2014. Designing of a box girder against distortion and torsional load [Finnish]. Bachelor's thesis. Lappeenranta: Lappeenranta University of Technology. 20 p.

Björk, T. 2014. Course handout. BK80A2302 Teräsrakenteet II. Lappeenranta: Lappeenranta University of Technology.

Björk, T. 2015. Doctor of Science in Technology; Professor of Steel Structures, Lappeenranta University of Technology. Private discussion 22.3.2015.

Fricke, W. 2013. IIW guideline for the assessment of weld root fatigue. Weld World, 57:753-791 p.

Haukaas, T. 2014. Warping Torsion [online]. Vancouver: University of British Columbia. Updated 30 March 2014 [cited 3 September 2014]. Available from http://www.inrisk.ubc.ca.

Hobbacher, A. 2013. Recommendations for fatigue design of welded joints and components. IIW document XIII-2460-13/XV-1440-13. Paris: International Institute of Welding. 163 p.

Kähönen, A. & Niemi, E. 1986. Distortion of a double symmetric box section subjected to eccentric loading – using the beam on elastic foundation approach. Lappeenranta: Lappeenranta University of Technology. ISBN 951-763-389-0. 37 p.

Martikainen, L. 2010. Kylmämuovatut teräsrakenteet. In: Kaitila, O et al. Teräsrakenteiden suunnittelu ja mitoitus Eurocode 3 -oppikirja. Helsinki: Teräsrakenneyhdistys. ISBN 978-952-9683-50-5. 140-149 p.

Murín, J. 2008. An effective finite element for torsion of constant cross-sections including warping with secondary torsion moment deformation effect. Slovak Republic: Slovak University of Technology. Engineering Structures 30, 2716-2723 p.

Murray, N. W. 1986 [1984]. Introduction to the Theory of Thin-Walled Structures. New York: Oxford University Press. ISBN 0-19-856186-5. 447 p.

Nethercot, D. A. & Salter, P. R. 1989. Design of Members Subject to Combined Bending and Torsion. Ascot [Berkshire]: The Steel Construction Institute. ISBN 1-870004-44-2. 120 p.

Pennala, E. 2002 [1994]. Lujuusopin perusteet. 11th edition. Helsinki: Otatieto. ISBN 951-672-297-0. 400 p.

Rautaruukki & Suomen Metalliteollisuuden Keskusliitto. 1987. Kylmämuovatut profiilit. Finland: Metalliteollisuuden Kustannus. ISBN 951-817-349-4. 248 p.

SFS-EN 1993-1-1. 2005. Eurocode 3: Design of steel structures - Part 1-1: General rules and rules for buildings. English version. Helsinki: Finnish standards association. 91 p.

SFS-EN 10219-2. 2006. Cold formed welded structural hollow sections of non-alloy and fine grain steel. Part 2: tolerances, dimensions and sectional properties. English version. Helsinki: Finnish standards association. 36 p.

Timoshenko, S. 1983 [1956]. Strength of Materials, part 2, advanced theory and problems. 3. edition. Malabar [Florida]: Robert E. Krieger publishing company. 572 p.

Rubin, H. 2005. Wölbkrafttorsion von Durchlaufträgern mit konstantem Querschnitt unter Berücksichtigung sekundärer Schubverformungen. Stahlbau 74, Heft 11. 826-842 p.

Rubin, H. 2007. Torsions-Querschnittswerte für rechteckige Hohlprofile nach EN 10210-2:2006 und EN 10219-2:2006. Stahlbau 76, Heft 1. 21-33 p.

Dimensions: Overall dimensions, wall thickness, Center line corner radius

$H := 150 \qquad B := 150 \qquad t := 8 \qquad r := 2 \cdot t$

$h := H - t$

$b := B - t \qquad b' := \frac{b}{2} - r \qquad h' := \frac{h}{2} - r$

$A_m := h \cdot b - (4 - \pi) \cdot r^2 \qquad U := 2 \cdot [h + b - (4 - \pi) \cdot r]$

$\gamma_0 := 2 \cdot \frac{A_m}{U}$

$\omega'_y := \frac{h}{2} - \gamma_0$

$\omega_1 := \omega'_y \cdot b' = -153.726$

$\rho := \operatorname{atan}\left(\frac{b'}{h'}\right) \qquad L := \sqrt{(h')^2 + (b')^2}$

$c_1 := (r - \gamma_0) \cdot r \qquad c_0 := \omega_1 + r \cdot b' + c_1 \cdot \rho \qquad c_2 := L \cdot r$

$\xi' := \operatorname{acos}\left(\frac{-c_1}{c_2}\right) = 0.733 \qquad !!! \ \xi' =< \pi/2 - \rho \qquad \frac{\pi}{2} - \rho = 0.785$

$\max\omega := c_0 + c_1 \cdot \xi' + c_2 \cdot \sin(\xi') = 154.883$

$\omega'_z := \gamma_0 - \frac{b}{2}$

$\omega_2 := \omega'_z \cdot h' = 153.726$

$\xi_1 := -\rho \qquad \xi_2 := \frac{\pi}{2} - \rho$

$\omega_s(\xi) := c_0 + c_1 \cdot \xi + c_2 \cdot \sin(\xi)$

Warping constant:

$I_{\omega 01} := \frac{1}{3} \cdot \omega_1^2 \cdot b' \cdot t \qquad I_{\omega 12} := \int_{\xi_1}^{\xi_2} (\omega_s(\xi))^2 \cdot t \cdot r \, d\xi \qquad I_{\omega 23} := \frac{1}{3} \cdot \omega_2^2 \cdot h' \cdot t$

$I_\omega := 4 \cdot (I_{\omega 01} + I_{\omega 12} + I_{\omega 23}) = 3.78 \times 10^7$

Secondary torsion constant:

Distance 0-1

$\Delta S_1 := \frac{1}{2} \cdot \omega_1 \cdot b' \cdot t$

$$J_{01} := \frac{1}{6}\cdot\Delta S_1\cdot b'\cdot h$$

$$f(\xi) := r\cdot t\cdot\left(c_0\cdot\xi + \frac{1}{2}\cdot c_1\cdot\xi^2 - c_2\cdot\cos(\xi)\right)$$

$$\Delta S'_1 := \Delta S_1 - f(\xi_1)$$

$$\Delta S_2 := \Delta S'_1 + f(\xi_2)$$

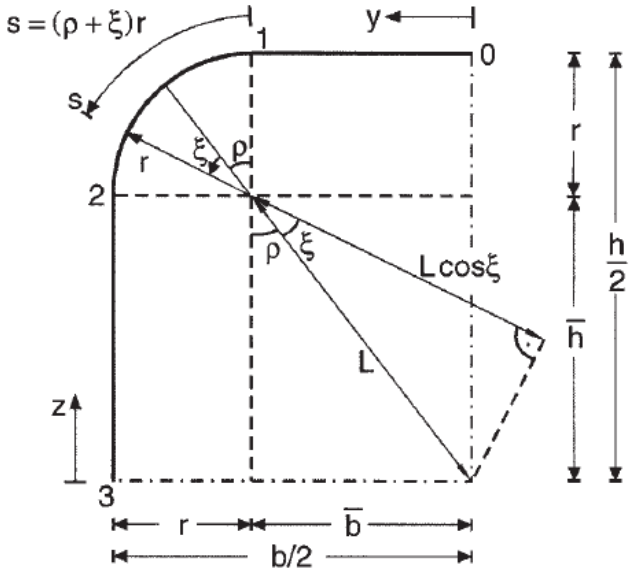

Distance 2-3

$$\Delta S_{23} := \frac{1}{2}\cdot\omega_2\cdot h'\cdot t$$

$$\Delta S_3 := \Delta S_2 + \Delta S_{23}$$

$$J_{23} := \left(\Delta S_3 - \frac{1}{3}\cdot\Delta S_{23}\right)\cdot\frac{b}{2}\cdot h'$$

Distance 1-2

$$J_{12} := \frac{1}{4}\cdot\Delta S'_1\cdot U\cdot r + r^3\cdot t\cdot\left[\left(\frac{1}{2}\cdot c_0\cdot\xi_2^2 + \frac{1}{6}\cdot c_1\cdot\xi_2^3 - c_2\cdot\sin(\xi_2)\right) - \left(\frac{1}{2}\cdot c_0\cdot\xi_1^2 + \frac{1}{6}\cdot c_1\cdot\xi_1^3 - c_2\cdot\sin(\xi_1)\right)\right] \ldots$$
$$+ r^2\cdot L\cdot t\cdot\left[\left[\left(c_0\cdot\xi_2 + c_1\cdot\frac{\xi_2^2 - 2}{2}\right)\cdot\sin(\xi_2) + (c_0 + c_1\cdot\xi_2)\cdot\cos(\xi_2) - \frac{1}{4}\cdot c_2\cdot(2\cdot\xi_2 + \sin(2\cdot\xi_2))\right] \ldots\right.$$
$$\left.+ -\left[\left(c_0\cdot\xi_1 + c_1\cdot\frac{\xi_1^2 - 2}{2}\right)\cdot\sin(\xi_1) + (c_0 + c_1\cdot\xi_1)\cdot\cos(\xi_1) - \frac{1}{4}\cdot c_2\cdot(2\cdot\xi_1 + \sin(2\cdot\xi_1))\right]\right]$$

$$S_0 := \frac{I_\omega + 4\cdot(J_{01} + J_{12} + J_{23})}{2\cdot A_m}$$

$$S_1 := S_0 - \Delta S_1 \qquad S_2 := S_0 - \Delta S_2 \qquad S_3 := S_0 - \Delta S_3 \qquad S'_1 := S_0 - \Delta S'_1$$

$$K_{01} := \int_0^{b'}\left(S_0 - \frac{1}{2}\cdot\omega'_y\cdot t\cdot y^2\right)^2 dy$$

$$K_{12} := \int_{\xi_1}^{\xi_2} \left(S'_1 - f(\xi)\right)^2 \cdot r \, d\xi = 1.424\times 10^{10}$$

$$K_{23} := \int_{0}^{h'} \left(S_3 + \frac{1}{2}\cdot\omega'_z \cdot t \cdot z^2\right)^2 dz$$

Sectorial warping static moments at specific locations:

$S_0 = -1.666\times 10^4$ $S_1 = 1.716\times 10^4$ $S_2 = 1.716\times 10^4$ $S_3 = -1.666\times 10^4$

NB: Only for square profile. Max sectorial (warping) static moment: $S_{max} := S_0 - \left(\Delta S'_1 + f(0)\right) = 2.731\times 10^4$

$$I_{Ts} := \frac{I_\omega^{\,2}\cdot t}{4\cdot\left(K_{01} + K_{12} + K_{23}\right)} = 9.986\times 10^4 \qquad I_\omega = 3.78\times 10^7$$

$$I_T := 4\cdot\frac{A_m^{\,2}}{U}\cdot t = 2.355\times 10^7$$

Reduced torsional constant EN 10210-2 ja 12019-2: $I_t := I_T + \frac{1}{3}\cdot U\cdot t^3 = 2.364\times 10^7$

$$\kappa := \frac{1}{1 + \frac{I_t}{I_{Ts}}} \qquad lo := \sqrt{\frac{2.6 I_\omega}{\kappa\cdot I_t}} \qquad Mt := 9456064 = 9.456\times 10^6$$

Bimoment Mw $Mw := \kappa\cdot lo\cdot Mt$

Primary torsional moment: $M_{Tp} := (1-\kappa)\cdot Mt$

Secondary torsional moment: $M_{Ts} := \kappa\cdot Mt$

Max primary warping stress: $max\sigma w := \frac{Mw}{I_\omega}\cdot max\omega = 5.123$

Primary shear stress: $\tau_p := \frac{M_{Tp}}{2\cdot A_m\cdot t} = 29.508$

Max secondary shear stress: (for square section only!) $max\tau_s := \frac{M_{Ts}}{I_\omega\cdot t}\cdot S_{max} = 3.591$

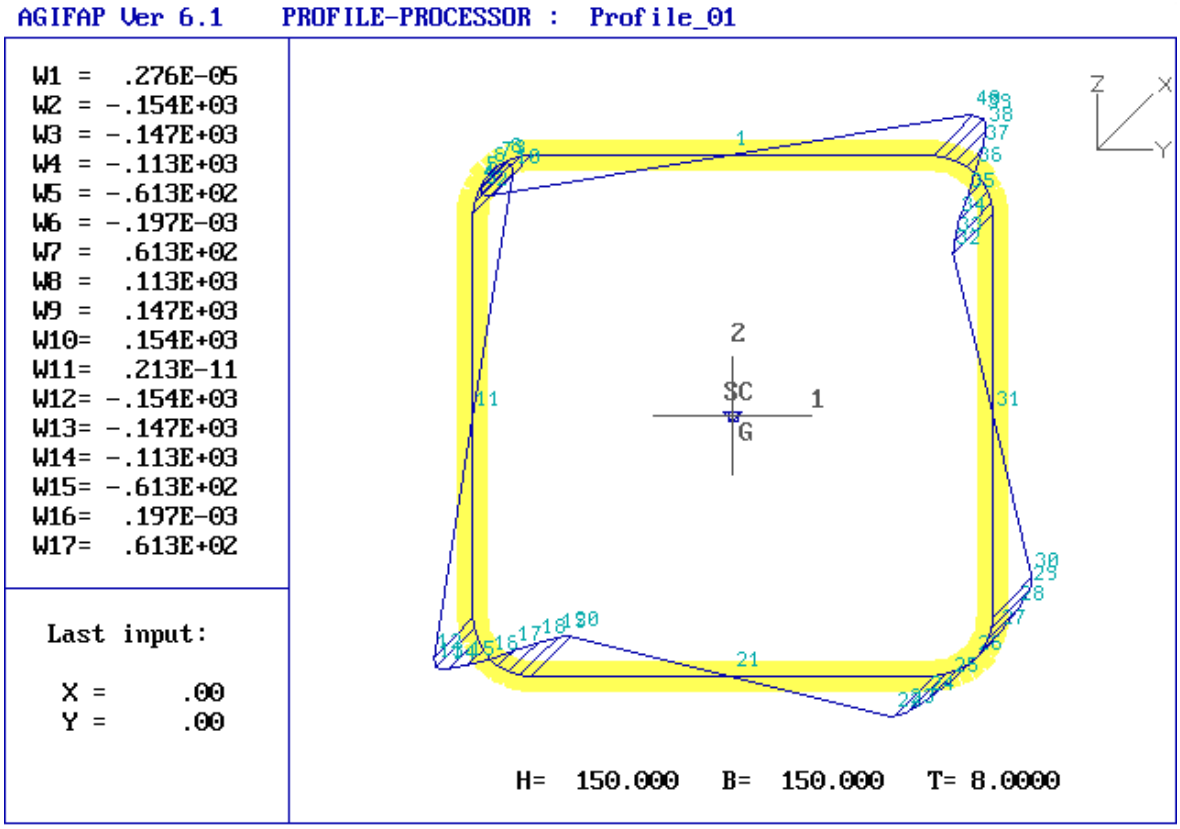

Figure 1. Warping function in the square structural hollow section.

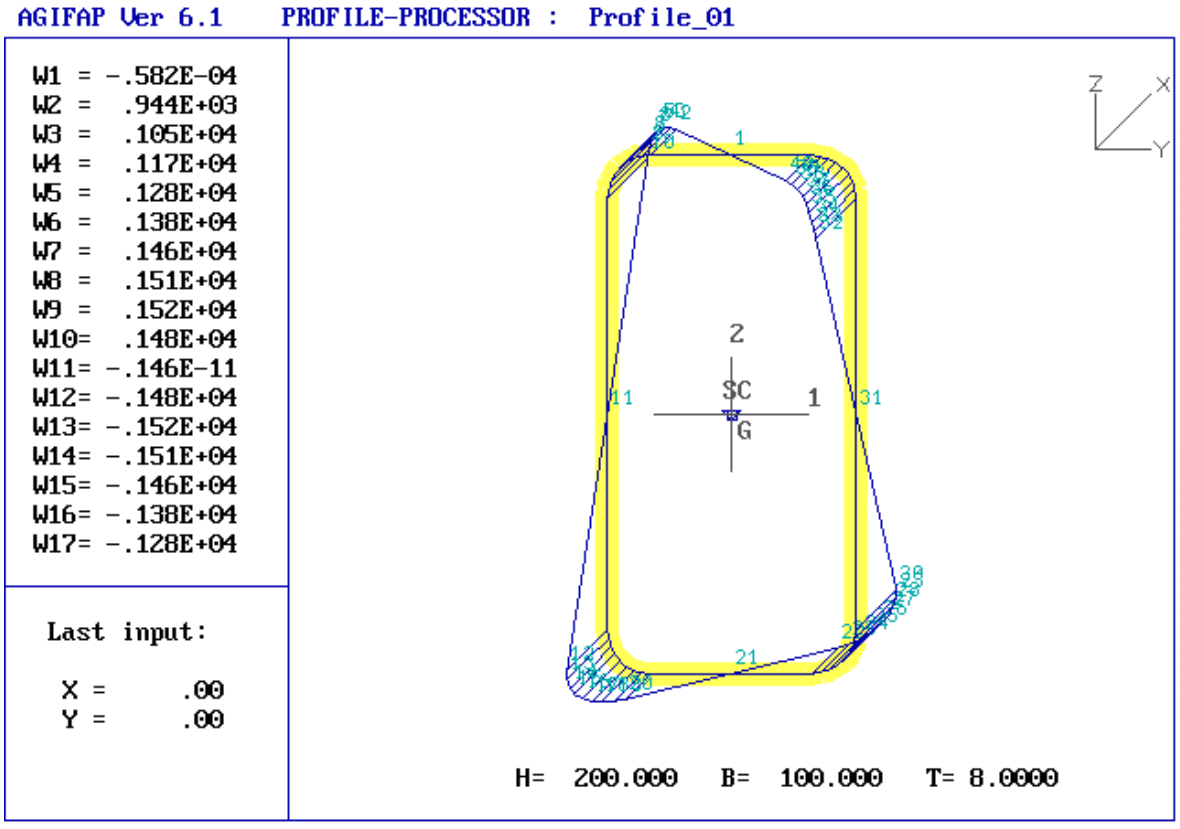

Figure 2. Warping function in the rectangular structural hollow section.